

Submitted to *J. Geophys. Res.-Atmospheres* V – 2 Oct 2017

First Reprocessing of Southern Hemisphere Additional Ozonesondes (SHADOZ) Ozone Profiles (1998-2016). 2. Comparisons with Satellites and Ground-based Instruments

Anne M. Thompson¹ and Jacquelyn C. Witte^{1,2} (¹Earth Sciences Division, NASA Goddard Space Flight Center, Greenbelt, MD 20771; 301-614-5905; anne.m.thompson@nasa.gov)
(²SSAI at NASA, Greenbelt, MD), Chance Sterling,^{3,4} Allen Jordan,^{3,4} Bryan J. Johnson,³ Samuel J. Oltmans,^{3,4}; Masatomo Fujiwara,⁵ Holger Vömel,⁶ Marc Allaart,⁷ Ankie Piters,⁷ Gert J. R. Coetzee,⁸ Francoise Posny,⁹ Ernesto Corrales,¹⁰ Jorge Andres Diaz,¹⁰ Christian Félix,¹¹ Ninong Komala,¹² Nga Lai,¹³ Matakite Maata,¹⁴ Francis Mani,¹⁴ Zamuna Zainal,¹⁵ Shin-ya Ogino,¹⁶ Francisco Paredes,¹⁷ Tercio Luiz Bezerra Penha,¹⁸ Francisco Raimundo da Silva,¹⁸ Sukarni Sallons-Mitro,¹⁹ Henry B. Selkirk^{1,20} F. J. Schmidlin,²¹ Rene Stuebi,¹¹ Kennedy Thiongo²²

RUNNING HEAD: Thompson et al.: SHADOZ Data Evaluation

Index Terms: 0368, 3314, 3360, 3362, 3374

Keywords: Ozone, ozonesondes, OMI, OMPS, SHADOZ, Tropical tropopause Layer

KEY POINTS:

Data from 14 long-term SHADOZ station have been reprocessed according to best practices to correct for ozonesonde instrument variability.

Comparisons of total column ozone among reprocessed sonde data, satellite and ground-based instruments agree within 2% for 12 of 14 stations.

In the tropics the 10-station data bias among stratospheric ozone profiles has been markedly reduced and a tropospheric wave-one remains.

Affiliation & Contact Information

Anne M. Thompson¹

1 NASA Goddard Space Flight Center, Earth Sciences Division, Greenbelt, MD 20771; 301-614-5905;

anne.m.thompson@nasa.gov CORRESPONDING AUTHOR

2 SSAI, Lanham, MD 20706; 301-614-5991; jacquelyn.witte@nasa.gov

Chance Sterling^{3,4}, Allen Jordan,^{3,4} Bryan J. Johnson³, Samuel J. Oltmans^{3,4}

3 NOAA ESRL, Global Monitoring Div., 325 Broadway, Boulder, CO 80305; 303-497-6676;

Chance.sterling@noaa.gov; allen.jordan@noaa.gov; Bryan.johnson@noaa.gov; samuel.j.oltmans@noaa.gov

4 Also at CIRES (Univ of Colorado Cooperative Institute, Boulder, CO 80302)

5 Faculty of Environmental Earth Science, Hokkaido University, Sapporo 060-0810 Japan; Tel: +81-11-706-2362, Fax: +81-11-706-4865; fuji@ees.hokudai.ac.jp

6 Earth Observations Laboratory, NCAR, Box 3000, Boulder CO 80307; voemel@ucar.edu

7 KNMI (Royal Dutch Meteorological Institute) de Bilt, PO Box 201. NL-3730 AE De Bilt Netherlands. OR Utrechtseweg 297. NL-3731 GANetherlands, marc.allaart@knmi.nl; ankie.piters@knmi.nl

8 South Africa Weather Service, Private Bag X097, Pretoria, South Africa; gerrie.coetzee@weathersa.co.za

9 Laboratoire de l'Atmosphère et des Cyclones (LACy), UMR8105 (Université, Météo-France,CNRS), La Réunion, France; Francoise.posny@univ-reunion.fr

10 Director of the Costa Rican National Hangar for Airborne Research Div. National Center for High Technology(CENAT) and Head, Gas Sensing Lab., Universidad de Costa Rica, San Jose, Costa Rica.

ernestocor@gmail.com; Jorge.andres.diaz@gmail.com

11 Federal Office of Meteorology and Climatology, MeteoSwiss, Aerological Station, P.O. Box 316, CH-1530

Payerne, Switzerland; +41 26 662 62 29; Christian.felix@meteoswiss.ch; rene.stuebi@meteoswiss.ch

12 National Institute of Aeronautics and Space (LAPAN), Jl. Dr. Djunjdunan 13., Bandung 40173, Indonesia;

Tel: 62-22-6037445; Fax: 62-22-6037443; ninongk@yahoo.com

13 Ngo Lai, Aero-Meteorological Observatory, National Hydro-Meteorological Service No.8, Phao Dai Lang Street, Dong Da District, Hanoi, Vietnam; Fax: +84 4 3835 8902; ltnga0171@gmail.com

14 The University of the South Pacific, Division of Chemistry - School of Biological and Chemical Sciences

Suva, Fiji; 679 313900 Ext. 2847; Fax: 679 302548; maata_m@usp.ac.fj; fmani@usp.ac.fj

- 15 Malaysian Meteorological Department, Ministry of Science, Technology and Innovation,
Jalan Sultan, 46667 Petaling Jaya, Selangor D.E, Malaysia; zamuna@met.gov.my
- 16 Japan Agency for Marine-Earth Science and Technology, Research Institute for Global Change, Tropical
Climate Variations Research Program, Monsoon Hydrological Cycle Research Team, 2-15 Natsushima-cho,
Yokosuka 237-0061, Japan Tel: 81-46-867-9263; Fax: 81-46-867-9255; ogino-sy@jamstec.go.jp
- 17 F. Paredes. Instituto Nacional de Meteorología y Hidrología, Ecuador, fparedes@inamhi.gob.ec
- 18 INPE, Brazilian Institute of Space Research, Laboratory of Environmental and Tropical Variables, Natal,
Brazil; terciolbp@crn.inpe.br; fraimundo@crn.inpe.br; terciolbp@crn.inpe.br
- 19 Meteorological Service of Suriname, Magnesiumstraat 41, Paramaribo, Suriname, +597 492980
sukarnimitro@yahoo.com
- 20 Also at Univ Space Research Associates, Columbia, MD; henry.b.selkirk@nasa.gov; 301-614-5046
- 21 NASA/GSFC/Wallops Flight Facility, Wallops Island, VA 23337; 757-824-1618;
francis.j.schmidlin@nasa.gov
- 22 Kenya Meteorological Department, Ngong Road, Dagoretti Corner, P. O. Box 30259 - 00100
Nairobi, Kenya; Tel: (+254) 20 3867880-5; Fax: (+254) 20 3876955 / 3877373. Kk_thiongo@yahoo.com

Abstract. The SHADOZ network was assembled to validate a new generation of ozone-monitoring satellites and to better characterize the vertical structure of tropical ozone in the troposphere and stratosphere. Beginning with nine stations in 1998, more than 7000 ozone and P-T-U profiles are available from 14 SHADOZ sites that have operated continuously for at least a decade. We analyze ozone profiles from the recently reprocessed SHADOZ dataset that is based on adjustments for inconsistencies caused by varying ozonesonde instruments and operating techniques. First, sonde-derived total ozone column amounts are compared to the overpasses from the EP/TOMS, OMI and OMPS satellites that cover 1998-2016. Second, characteristics of the stratospheric and tropospheric columns are examined along with ozone structure in the tropical tropopause layer (TTL). We find that: (1) Relative to our earlier evaluations of SHADOZ data, in 2003, 2007 and 2012, sonde-satellite total ozone column offsets at 12 stations are 2% or less, a significant improvement. (2) As in prior studies, the ten tropical SHADOZ stations, defined as within ± 19 degrees latitude, display statistically uniform stratospheric column ozone, 229 ± 3.9 DU, and a tropospheric zonal wave-one pattern with a 14 DU mean amplitude. (3) The TTL ozone column, which is also zonally uniform, masks complex vertical structure; this argues against using satellites for lower stratospheric ozone trends. (4) Reprocessing has led to more uniform stratospheric column amounts across sites and reduced bias in stratospheric profiles. As a consequence the variability in total column ozone now averages 5%.

1
2
3
4
5
6
7
8
9
10
11
12
13
14
15
16
17
18
19
20
21
22
23
24
25
26
27
28
29
30

1. INTRODUCTION

1.1. Design and Features of the SHADOZ Network

The Southern Hemisphere Additional OZonesonde network (SHADOZ; refer also to *Acronym List* below) was initiated in 1998 as an international partnership with both technological and scientific goals that required augmenting the number of tropical ozone soundings in the troposphere and stratosphere [Thompson *et al.*, 2003a; 2011a,b; 2012]. The ozonesonde data are collected from electrochemical concentration cell (ECC) type [Komhyr, 1969] sensors launched with a standard radiosonde. Details of ozonesonde-radiosonde pairings used at SHADOZ stations are given in the archival papers [Thompson *et al.*, 2003a, hereafter referred to as T03; Thompson *et al.*, 2003b; Thompson *et al.*, 2007, hereafter referred to as T07; Thompson *et al.*, 2012, hereafter referred to as T12] and in the companion paper to this one [Witte *et al.*, 2017a; referred to hereafter as Witte17a].

The original spatial coverage of SHADOZ was determined by two requirements: (1) that the network consist of existing stations; and (2) full zonal coverage to resolve an equatorial “wave-one” feature observed in satellite total ozone [Fishman and Larsen, 1987; Shiotani, 1992; Kim *et al.*, 1996; Thompson *et al.*, 2000; T03; Thompson *et al.*, 2003b; Sauvage *et al.*, 2006]. At the initiation of SHADOZ in 1998 there were nine stations meeting these criteria, all in the southern hemisphere, hence the name of the network [T03]. Stations north of the equator joined SHADOZ as follows: Kuala Lumpur (in 1999; Yonemura *et al.*, [2002]); Paramaribo (1999 [Peters *et al.*, 2004; Fortuin *et al.*, 2007]); Costa Rica (in 2005; Selkirk *et al.*, 2010); Cotonou (operated 2004-2007; Thouret *et al.*, 2009); Hanoi, where soundings began in 2004 [Ogino *et al.*, 2013]. Hilo, Hawaii, with a record extending back to the 1980s, joined SHADOZ in 2009. The 14 stations that have operated at least a decade during SHADOZ and that are covered in this paper, appear in **Figure 1**. More than 7000 sets of ozone and pressure-temperature-humidity (PTU) profiles from a total of 17 stations that have been part of SHADOZ and are available at the website: <<https://tropo.gsfc.nasa.gov/shadoz>>.

For the first 10-15 years of SHADOZ the data were used principally in three ways. First the profiles were used to create climatologies for satellite algorithms [McPeters *et al.*,

31 2007; *McPeters and Labow, 2012; Labow et al. 2015*], to evaluate chemical-transport
32 models [*Martin et al. 2002; Stevenson et al., 2006; Kaminski et al. 2008*] and as a reference
33 for coupled chemistry-climate models [*Eyring et al., 2005*] in intercomparison exercises
34 that support UNEP/WMO Ozone [*WMO, 2007; 2011; 2014*] and the IPCC 2007 Assessment.
35 Statistical approaches have been used to create more geographically coherent
36 climatologies [*T12; Tilmes et al., 2012; G. Liu et al., 2013; J. Liu et al., 2013*]. Self-organizing
37 maps of sondes, in particular, capture meteorological and chemical impacts on profile
38 structure [*Jensen et al. 2012; Stauffer et al., 2016*].

39 Second, ozone structure near the tropopause has been studied, in the so-called
40 “tropopause transition layer” or “tropical tropopause layer” (TTL; *Folkins et al., 2002;*
41 *Takashima and Shiotani, 2007*), with ozone-water vapor relationships captured in the
42 relatively high-accuracy hygrometer data for H₂O [*Fujiwara et al., 2001; Vömel et al., 2002*].
43 Signatures of convection, waves, and climate oscillations (ENSO, QBO) dominate ozone
44 interannual variability in the free troposphere (FT) and lower stratosphere (LS). *Selkirk et*
45 *al. [2010]* and *Thompson et al. [2010]* quantified wave impacts on Costa Rican sondes
46 launched during the Tropical Composition, Clouds and Chemical Coupling (TC⁴) campaign.
47 At Ascension, even though convection is less prevalent than over the western Pacific and
48 Indian Oceans, profiles with the lowest mean tropospheric ozone mixing ratio display an S-
49 shape year-round [T12]. This is presumably a combination of the regional subsidence
50 along with convection in some months (Figures 4 and 8 in T12; Figure 4 in *Jensen et al.,*
51 *[2012]*). In *Thompson et al. [2011a]* gravity waves were identified through ozone laminae
52 within the upper troposphere (UT) and TTL. A gravity-wave index constructed for 12
53 SHADOZ stations captured responses to ENSO episodes.

54 Third, satellites use SHADOZ profiles for validation of tropospheric and/or
55 stratospheric data (e.g., Aura validation; Special Issue of *J. Geophys. Res.*, 2007-2008) and
56 newer sensors like OMPS on Suomi-NPP, IASI and GOME-2 (**Figure 2**). SHADOZ data have
57 also been used to derive ozone trends [*Heue et al., 2016*]. In *Randel and Thompson [2011]* a
58 composite SAGE II and SHADOZ dataset (1984-2009) for ozone over eight equatorial
59 stations, defined a lower stratosphere (LS) trend of -(2-4)%/decade. Two subtropical
60 sounding stations with data prior to the start of SHADOZ, Irene and La Réunion, displayed
61 large positive trends in FT ozone, not in summer or spring, when biomass fires are

62 widespread, but in winter [Thompson *et al.*, 2014]. In Gebhardt *et al.* [2014], combined
63 SCIAMACHY and SHADOZ data for 2002 to 2012 show flat to slightly increasing ozone in
64 the equatorial LS. Hubert *et al.* [2016] employed sonde profiles to evaluate satellite drift
65 over the past 10-15 years. To date, it appears that most operational satellites (14 limb
66 sounders were evaluated by Hubert *et al.*, [2016]) are quite stable in the lower and middle
67 stratosphere. To be used as references for satellite drift evaluation, the sonde precision
68 needs to be 3-5%, somewhat better than the level achieved in the past 10-15 years.

69 **1.2 Quality Assurance: Technological Aspects of SHADOZ**

70 An essential technological goal of SHADOZ is to adopt, when appropriate,
71 recommendations for sonde technique and data processing when researchers have used
72 laboratory and field test results to produce consensus-based recommendations for data
73 handling. The beginning of SHADOZ coincided with a series of JOSIE (Jülich [Germany]
74 Ozonesonde Intercomparison Experiments) in test chambers [Smit and Kley, 1998; Smit
75 and Straeter, 2004], as well as laboratory studies elsewhere [Johnson *et al.*, 2002]. ECC
76 ozonesonde manufacturers modify materials from time to time [Komhyr, 1986; Komhyr *et*
77 *al.*, 1995] and several variations of the potassium iodide sensing solution that reacts with
78 ozone molecules are widely used [Witte17a]. Furthermore, the motor-driven Teflon piston
79 pump that draws air into the cells of the ECC instrument drops in efficiency as the sonde
80 ascends into the stratosphere. Several groups have employed different formulae to correct
81 for this effect, in a “pump efficiency correction factor” or PCF. Thus, different combinations
82 of instrument manufacturer, sensing solution type (SST) and PCF can lead to divergent
83 values of ozone partial pressure. These variations prompted the World Meteorological
84 Organization (WMO) to support the formation of the World Ozonesonde Calibration
85 Chamber System [Smit and Kley, 1998] in Jülich, and, starting in 1996, to sponsor the JOSIE
86 series of chamber tests. In JOSIE experiments to date, different types of sondes, not all of
87 them ECC, measured ozone introduced into the chamber at changing temperatures and
88 pressures that simulate a balloon ascent to 10 hPa. A UV photometer [Profitt and
89 McLaughlin, 1983] supplies the reference ozone measurement to which the sonde reading
90 is compared.

91 The JOSIE-2000 campaign [Smit *et al.*, 2007] accommodated SHADOZ by testing
92 combinations of instrument type and SST in chamber simulations that followed the

93 temperature and typical ozone trace of a tropical sounding. Clear biases from differences
94 in the instrument manufacture (there are basically two ECC hardware types) and SST were
95 apparent. In 2004 the BESOS field campaign, conducted in Wyoming USA, with a standard
96 UV photometer and a gondola of 18 ozonesondes on a large balloon, displayed similar
97 biases among sonde types [Deshler *et al.*, 2008]. These intercomparison activities led to
98 recommendations of certain ozonesonde instrument-SST combinations for more consistent
99 sonde results and served as the basis for WMO/GAW standard operating procedures [Smit
100 and ASOPOS, 2014]. Several SHADOZ stations modified their technique and/or reprocessed
101 data during the period 2000-2005, improving agreement between total ozone values from
102 the sondes and co-located ground-based instruments and total ozone satellite instruments
103 [T07; T12] relative to the first comparisons in T03. JOSIE and related activities have
104 reduced the total uncertainty of the sonde measurement from ~15-20% to 5-10% [WMO,
105 2007; 2011]. Nonetheless, SHADOZ total ozone column amounts referenced to satellite
106 (TOMS or OMI) columns as well as stratospheric ozone columns from the sondes indicated
107 station-to-station biases [T07; T12]. Some of the biases followed discrepancies associated
108 with variations in SST and instrument that were identified in JOSIE and BESOS.

109 **1.3 Ozonesonde Reprocessing: Goals of this Study**

110 Since 2010, workshops of the SI2N (SPARC-IO3C-IGACO-NDACC) activity and a
111 series of Ozonesonde Experts Meetings have led to recommendations on how to reprocess
112 soundings to compensate for the range of instrument type, SST, and various choices of
113 background current and PCF [Smit and ASOPOS, 2012]. An important element of
114 reprocessing data from different SST and ozonesonde instruments is to homogenize data
115 with a “transfer function.” Deshler *et al.* [2017] supply transfer functions for the major
116 combinations of instrument type and SST. At present 6-8 providers of ozonesonde data,
117 representing ~30 stations globally, have adopted the guidelines. Papers describing the
118 reprocessing of Canadian network data [Tarasick *et al.*, 2016] and two European records
119 [Van Malderen *et al.*, 2016] have appeared. In the past two years we have been
120 reprocessing the SHADOZ profiles for 14 stations that have records of at least 10 years
121 within the period 1998-2016. The basis for the reprocessing is Smit and ASOPOS [2012]
122 with some modification for several stations as described in Section 2. Details for the
123 reprocessing of data from the first seven stations appear in Witte17a. Additional

124 reprocessing, including for an 8th station, are given, along with ozone profile and column
125 uncertainties in J. C. Witte et al., First reprocessing of Southern Hemisphere ADditional
126 Ozonesondes (SHADOZ) profile records: 3. Uncertainty in ozone profile and total column, *J.*
127 *Geophys. Res. Atmos.*, doi: 10.1002/2017JD027791, submitted, hereafter referred to as
128 Witte17b. The complete reprocessed SHADOZ dataset will be released as SHADOZ v6.0.
129 The present study evaluates the reprocessed data to date and addresses the following:

- 130 • How do total column ozone (TCO) amounts for the SHADOZ stations agree with
131 satellite TCO in the period 1998-2016? How do the sonde ozone columns compare
132 to co-located Dobson, Brewer, and SAOZ instruments at nine SHADOZ stations?
- 133 • How do stratospheric, tropospheric and TTL column ozone amounts for the
134 tropical stations (defined as within ± 19 degrees of the equator), calculated from
135 the reprocessed data, compare to one another? Are the stratospheric and TTL
136 ozone columns zonally uniform? What is the variability in TCO after reprocessing?
- 137 • What are tropospheric column ozone amounts at each station with the
138 reprocessed data? What is the magnitude of the wave-one pattern in tropospheric
139 ozone?
- 140 • Using a mean reference profile from the tropical SHADOZ stations, are there
141 station biases in stratospheric ozone? Have biases changed from T07 and T12?

142 We summarize operating characteristics of all SHADOZ stations (**Section 2**) and
143 present the results in **Section 3**. **Section 4** is a summary.

144

145 **2. DATA AND METHODS OF ANALYSIS**

146 **2.1 SHADOZ and other Ozone Instrumentation**

147 The 14 SHADOZ sites (**Figure 1**) launch 2-4 times/month mostly between 0800 and
148 1400 Local Time. **Table 1** presents station location and numbers of soundings that are
149 used in our analyses, along with independent total ozone instrumentation. The station
150 labeled as Costa Rica represents sonde launches near San Jose, the capital, that have
151 changed location several times since late 2005.

152 SHADOZ archives ozone profiles with records of temperature, pressure, and relative
153 humidity from standard radiosondes. Over the 19-year record covered here, Vaisala RS-80,

154 RS-92, MW-41 and Intermet (iMet) radiosondes have been used at most stations (**Table 2**).
155 Exceptions are Réunion, where a Meteo Modem radiosonde has been employed, and Kuala
156 Lumpur where various ozonesonde-radiosonde combinations appear with four different
157 radiosonde manufacturers. The Lockheed-Martin Sippican radiosonde, a successor to Viz,
158 is used at Natal and was employed at Ascension from 1998 through mid-2010. When
159 Ascension launches resumed in March 2016, EnSci ozonesondes replaced Science Pump
160 Corporation (SPC) instruments and an iMet radiosonde was used. Details of each station's
161 equipment are found at <<https://tropo.gsfc.nasa.gov/shadoz>>; every record's meta-data
162 lists instrument type and usually serial number for ozonesonde and radiosonde. Details of
163 the SHADOZ radiosonde/ozonesonde systems for seven stations appear in Witte17a. In the
164 case of Watukosek, only data from mid-2001, taken using Strato software with EnSci ECC
165 and RS80 sondes have been reprocessed (reprocessing of 1999-2001 EnSci/RS-80 data
166 with a V03 data system is pending). Hilo, Fiji, Samoa and San Cristóbal sondes, reprocessed
167 by C. Sterling and B. J. Johnson (*Personal Communication*, 2017; reprocessing method
168 referred to as Sterling17 in **Table 1**), switched from Vaisala RS-80 radiosondes to iMet or
169 RS-92 after 2010. **Table 2** shows the time period of each radiosonde at the nine stations
170 where there have been changes. For comparisons with satellite and ground-based total
171 ozone instruments, data compromised by balloon bursts lower than 15 hPa are not used.
172 Above 10 hPa or burst, extrapolation to total column is made with the climatology of
173 *McPeters and Labow* [2012]. No normalization to the total ozone reading of a satellite or
174 ground-based instrument is made. Ground-based data are taken from the WOUDC and
175 NDACC public archives.

176 Sonde total ozone comparisons are made with satellite measurements from three
177 instruments of similar design that operated in the 1998-2016 period (**Figure 2**). These
178 are: NASA's Earth Probe/TOMS (Total Ozone Mapping Spectrometer) instrument, covering
179 sonde launches from January 1998-September 2004; the Dutch/Finnish OMI (Ozone
180 Monitoring Instrument) on board NASA's Aura spacecraft (September 2004 to the
181 present); OMPS (Ozone Mapping Profiler Suite) on the NASA-NOAA Suomi-National Polar-
182 orbiting Partnership from February 2012 to the present. In the latter period both OMI and
183 OMPS overpass total ozone are used; there are more OMPS measurements because of post-
184 2008 degradation in the OMI detector array. Not every sonde record is evaluated with the

185 satellite because overpass data are screened for cloudiness greater than 60% and the
186 satellite distance is limited to < 200 km.

187 2.2 Reprocessed Ozonesonde Data

188 A summary and reference for the reprocessing of each station appears in **Table 1**.
189 Details for seven stations that were reprocessed at NASA/Goddard appear in Witte17a:
190 Natal, Ascension, Irene, La Réunion, Kuala Lumpur, Hanoi, and Watukosek (**Figure 1**). In
191 Witte17a, comparisons of sonde total ozone for 1998-2015 with TOMS and OMI satellites
192 are made with original (SHADOZ version 5.2) and reprocessed data to demonstrate
193 improvements in the satellite-sonde offset. Also in Witte17a mid-stratospheric ozone from
194 the sonde profiles before and after reprocessing is compared to coincident Aura/MLS data
195 from September 2004 through 2015. Notable improvements appear between 65 hPa and
196 10 hPa for six of the seven stations. Since Witte17a was completed, we added all the 2016
197 reprocessed SHADOZ data to our seven-station reprocessing and completed reprocessing
198 of Nairobi data [Witte17b]. Witte17a has since reprocessed Costa Rica data in the same
199 way. A transfer function, developed by *Deshler et al.* [2017], was applied to the La Réunion
200 data after 2007 to correct for a solution change. These data are now homogenized to an
201 EnSci/0.5%, half buffer SST [Witte17b].

202 The four stations with data reprocessed by the NOAA ESRL/GMD Ozone group
203 (Hilo, Samoa, San Cristóbal, Fiji) used a 2.0% unbuffered SST with EnSci's for the 1998-
204 2005 period, after which they switched to a 1.0% 1/10th buffer SST (Sterling17, **Table 1**).
205 The 1998-2005 data have been reprocessed in the same way as the Watokusek data that
206 are based on the EnSci/2.0% unbuffered SST [Witte17a]. A transfer function based on
207 *Deshler et al.* [2017] is applied to the San Cristóbal 1998 - 2006/11/02 data to convert
208 ozone measurements made with a SPC/6A sonde to an EnSci/Z equivalent. This gives
209 roughly a 4% increase in the ozone profile measurements.

210 Paramaribo data have been reprocessed by KNMI (M. Allaart and A. Piters, *Personal*
211 *Communication*, 2017) according to the O3S-DQA [*Smit and ASOPOS*, 2012] guidelines;
212 where background currents required adjustment, the guideline of *Newton et al.* [2016] was
213 followed.

214 2.3 Analyses. Tropopause and TTL Definitions.

215 In the analyses that follow, we refer to the TTL and the tropopause, terms that
216 sometimes vary from one study to another. The TTL is defined as a region in which both
217 tropospheric and stratospheric properties are found in terms of constituent mixing ratios
218 and temperature gradients, wave activity, radiative heating rates and other thermodynamic
219 quantities [Gettelman and Forster, 2002; Fueglistaler et al., 2009]. We adopt 15-18.5 km for
220 the TTL (**Figure 3**) that encompass the minimum and maximum tropopause values for
221 tropical sites within 19 degrees of the equator. This range is ~1 km higher than Fueglistaler
222 et al. [2009]. However, our TTL definition encompasses the locations of the tropical cold-
223 point tropopause (CPT, Selkirk et al., [2010]), the thermal lapse-rate tropopause and the
224 ozonopause, i.e., an ozone tropopause defined as the height at which there is a sharp
225 gradient in ozone concentration at the base of the stratosphere [Bethan et al., 1996;
226 Sivakumar et al., 2011; T12]. We use the Bethan et al. [1996] definition for the tropopause.
227 The values in **Figure 3** are virtually identical for 10 stations, averaging 17.1 km, and there
228 are few tropopause heights below 14 km.

229

230 **3. Results and Discussion**

231 **3.1 Sonde Total Ozone Columns Compared to Ground-based Instrument and** 232 **Satellite Overpass Total Ozone**

233 For the 14 stations **Figure 4** shows a time-series of integrated total ozone from the
234 sonde (red) and the daily TOMS/OMI/OMPS overpass total. The order of the individual
235 panels is west to east by longitude, starting at 180W longitude. The satellite total ozone
236 from TOMS appears in dark gray, OMI total ozone is in black and OMPS total ozone is in
237 silver. For nine stations (**Table 1**) total column ozone from a co-located instrument, a
238 Brewer Spectrometer, a Dobson or SAOZ, is also shown in **Figure 4** (blue). The lower panel
239 of each time-series summarizes the ratio of sonde total ozone to the corresponding satellite
240 overpass or ground-based measurement. At the right in each figure there is a histogram of
241 offsets between the sonde total from the reprocessed data and the satellite (yellow). There
242 are five stations without ground-based total ozone instruments: Ascension, Hilo, San
243 Cristóbal, Costa Rica, and Fiji. For the nine stations with ground-based instruments, a
244 histogram of the sonde total and the ground-based instrument ozone total (hatched in
245 **Figure 4**) also appears in the right panel. Comparisons of total ozone from the ground-

246 based instrument and the concurrent satellites appear in **Figure 5**. In **Figure 4** sonde and
247 satellite comparisons display a high fraction of near-zero differences for every station
248 except two datasets where the distribution peaks are skewed closer to +5% (Paramaribo)
249 and -5% (Kuala Lumpur). All but two of the sonde-satellite discrepancies show the sonde
250 total to be lower than the satellite (**Table 3**), similar to prior SHADOZ satellite-sonde total
251 ozone comparisons [T03; T07; T12; Witte17a].

252 Among the 14 stations all but Kuala Lumpur and Paramaribo have an average
253 agreement with the satellite overpasses within 2% absolute or better (**Table 3**, column 4).
254 This represents a significant improvement over the sonde data currently archived, as
255 described in Witte17a (Table 4) and Sterling17. Overall, sonde-satellite agreement is
256 improved relative to the total ozone comparisons in T07 (EP/TOMS satellite reference, for
257 sondes launched in 1998-2004) and in T12 (Figure 11, for OMI comparisons, 2005-2009).

258 **3.1.1 Sonde-Satellite-Ground-based Time-series at Individual Stations**

259 Samoa is one station for which the total ozone agreement has improved considerably
260 since the T03 evaluation where the sonde-TOMS ozone offset, based on 1998-2000
261 soundings, was ~10%. For 1998-2004, with some instrument and sensing solution
262 changes after JOSIE-2000 [Smit *et al.*, 2007], satellite and Dobson comparisons implied that
263 the sondes were 5-7% too low [T07]. Reprocessing improves the satellite agreement on
264 average, from 1998-2016, to 0.9% mean difference (column 4 in **Table 3**). The Dobson
265 total ozone also agrees well with the sonde TCO. This is seen in the histograms in the right
266 panel of **Figure 4a** that display a relatively tight and Gaussian distribution of sonde-
267 satellite (yellow) and sonde-Dobson (hatched) total ozone.

268 Referring to the lower panel in **Figure 4a**, the sonde/TOMS ratio (1998-late 2004)
269 averages 0.97-0.98. There are other features to note with the Samoa data (**Figure 4a**).
270 First, the sonde/Dobson ratio for 1998-late 2004 is slightly higher than sonde/TOMS. This
271 implies that TOMS total ozone is greater than the Dobson; that is consistent with the
272 Dobson/TOMS ratio peaking at less than 1.0 in **Figure 5a** (yellow shading). Second, from
273 2006 through 2010 in the OMI period, the sonde/Dobson ratio and sonde/OMI are both
274 closer to 1.0 (**Figure 4a**) than the 1998-2004 sonde-Dobson-TOMS comparisons (T07).
275 This too agrees with the peaking of Dobson/OMI total ozone ratio peaking near unity in
276 **Figure 5a** (blue hatched). Third, the close sonde-satellite-Dobson agreement continues

277 into mid-2014, when most of the sonde-satellite comparisons are based on OMPS. The
278 ratios, both sonde/OMI and sonde/OMPS, declined on average from late 2014 through
279 2016. During OMPS there are many Dobson comparisons with the satellite (**Figure 4a**) but
280 few sonde comparisons with the Dobson. The Dobson/OMPS (green hatched in **Figure 5a**)
281 peaks slightly lower than the Dobson/OMI, but it is higher than Dobson/TOMS.

282 In **Figure 4b** for Hilo (elevation 10m), only satellite comparisons are displayed
283 because the nearby Dobson spectrometer at Mauna Loa is 3.4 km above mean sea level.
284 Hilo displays one of the best homogenized sonde records throughout the SHADOZ period.
285 Because of its northern sub-tropical location, there is a large variation in total ozone, close
286 to 100 DU in a highly regular cycle (see also Figure 10e in T12). Maximum total ozone over
287 Hilo from February to May [*Oltmans et al., 2004; T12*] during which the UT/LS displays
288 extratropical ozone-rich air and a lower tropopause (Figure 3b in T12). In contrast, July-
289 September are characterized by lower ozone throughout the free troposphere with a mid-
290 troposphere minimum that resembles boundary-layer Hilo ozone (Figure 3b in T12),
291 suggestive of convective mixing. The Hilo-satellite comparisons (**Figure 4b**) show similar
292 patterns to the Samoa (**Figure 4a**) sonde ratios. For the TOMS to early OMI period, 1998-
293 2005, the Hilo ratios average an equivalent of 1-2% lower ozone than the satellites (**Figure**
294 **4b**). After that, up through 2013, the sonde/satellite ratio clusters about 1.0, with nearly
295 all data within 0.95-1.05. In the first two years of the OMI-OMPS overlap the sonde-
296 satellite ratio resembles the 2004-2011 record. In mid-2014, as with Samoa, Hilo sonde
297 ratios decline several percent with a number of values falling below 0.9. This pattern is
298 reflected in the histogram of satellite to sonde offsets (yellow at right of **Figure 4b**). The
299 tail of negative values, corresponding to sonde lower than satellite, extends almost to -20%.
300 However, the overall sonde-satellite difference is -1.2% (**Table 3**, sonde lower).

301 In **Figure 4c** the San Cristóbal time-series displays several data gaps, e.g., no launches
302 in 2009-2011, with a drop in launch frequency in 2012-2015. The sonde/satellite ratios for
303 the TOMS and early OMI era (1998-2005) averages 0.93. As with Samoa and Hilo (**Figures**
304 **4a,b**), the sonde/OMI ratio for 2006-2008 exceeds 1.0 but in 2012-2015, the ratio drops to
305 ~0.95. The San Cristóbal histogram (right in **Figure 4c**) skews toward -20%, but 80% of
306 the differences are close to zero, averaging a -0.9% offset, i.e., sondes have lower ozone.

307 The Costa Rican sondes that started in 2005 (**Figure 4d**) span the OMI and OMPS
308 periods. They suggest a pattern somewhat different from the three Pacific stations
309 illustrated in **Figures 4a-c**. In 2005 through most of 2007 the ratio is frequently greater
310 than 1.0. From late 2007 through early 2015 ratios span 0.9 to 1.07, during which there
311 seem to be two distinct phases. From late 2007 through early 2014 the ratios are
312 predominantly less than 1.0, followed by many values > 1.0 after mid-2012 (note: more
313 statistics partly result from frequent OMPS overpasses). After 2014, although the
314 percentage of sonde/satellite ratios greater than 1.0 increases, the distribution shifts to
315 more values < 0.9 . In 2016 there are many sondes with ratios 0.80-0.90. The Costa Rica
316 histogram (right in **Figure 4d**) displays negative values to -20% but the overall mean
317 relative to OMI and OMPS is -0.2% (column 4, **Table 3**).

318 The sondes at Paramaribo (**Figure 4e**) represent the only reprocessed dataset for
319 which the sondes display markedly higher ozone than the satellites and the ground-based
320 instrument for most the period 1999-2016. Paramaribo is the SHADOZ station with the
321 second largest ground-based dataset; the Brewer/satellite ozone ratios in **Figure 5b** are
322 based on more than 5000 coincidences. Comparisons of Brewer total ozone with the three
323 satellites agree well; as for Samoa (**Figure 5a**), the ozone from the ground-based
324 instrument relative to the satellite varies among the three satellites at Paramaribo. TOMS
325 has highest ozone (lowest ratio, yellow in **Figure 5b**) with sonde/OMI somewhat higher
326 than sonde/OMPS. In **Figure 4e**, between 2011 and 2014 there is an almost monotonic
327 increase in the sonde/satellite ratios that disappears by 2015. These persistent positive
328 ratios, interpreted in the past as signifying a bias at Paramaribo relative to profiles of the
329 other 9 tropical stations (Figure 13b in T12), disappear after 2015. Then the sonde/
330 satellite (OMI and OMPS) and sonde/Brewer ratios more closely resemble the four stations
331 discussed above. Around 2015 there was a change in the sonde sensing solution; the data
332 are being reprocessed again (A. Piters and M. Allaart, *Personal Communication*, 2017).

333 The Natal record (**Figure 4f**) displays several data gaps; the hiatus from 2011 to early
334 2014 was due to equipment malfunction, then obsolescence. As with the Pacific and South
335 American stations (**Figures 4a-e**), agreement among sonde, satellites and Dobson total
336 ozone overall at Natal is very good (**Table 3**). The histogram of ratios (as % offset), right
337 frame in **Figure 4f**, averages -1.7% for the composite satellite record (yellow); the Dobson

338 appears to peak slightly lower (hatched in **Figure 4f**), skewing more negative than the
339 satellite-referenced offsets. Similar to the five stations discussed so far, there is a 2014-
340 2016 drop-off in sonde ratios, consistent among OMI/OMPS and Dobson, at Natal (**Figure**
341 **4f**), even though the instrumentation used at Natal differs from the other stations. The
342 Natal time-series during the TOMS period is unique, with many of the ratios starting out in
343 1999 and 2000 at 10% lower than the satellite and Dobson [T03, T07]. From late 2000
344 until early 2002, the sonde/TOMS corresponds to 3-4% positive; the sonde also increases
345 relative to the Dobson but mostly remains below 1.0. After early 2002 the sonde-Dobson
346 and TOMS ratios are nearly all below 1.0 again, values that persist to late 2004 to 2006 as
347 the satellite data transition from TOMS to OMI. In mid-2007 and throughout 2008 the
348 sonde ratios relative to both OMI and Dobson become largely >1.0. Natal has > 3300
349 Dobson-satellite coincidences (**Figure 5c**) with all three satellite ratios peaking near 1.0.

350 The instrumentation, preparation technique and data-processing for Ascension
351 (**Figure 4g**) were the same as at Natal from 1998-2010 when the Ascension launches were
352 suspended. Data from 2016 onward are provided by an Ensci/iMet combination instead of
353 LMS with SPC (**Table 2**). The sonde data at Ascension are fairly noisy and much of the
354 distribution of ratios is skewed to values < 0.90 (more negative than 10% in the histogram
355 in **Figure 4g**). Low ratios are prominent in the beginning of the record, from 1998 to late
356 2001. After that, from the late TOMS to early OMI period, 2002-2008, there is an increase
357 in the factors, to a majority at > 1.0. A short gap follows, after which the values drop to an
358 average ~0.95. After the longer gap, there is a tight clustering between 0.90 and 1.0
359 (histogram average ~-5%). The mean sonde-satellite offset is -2.4%.

360 There was a 4-plus year data gap in Irene (**Figure 4h**) largely due to equipment failure.
361 The sonde/satellite and sonde/Dobson ratios are similar; this is also seen in the histograms
362 at the right in **Figure 4h**. Most satellite offsets (yellow in the histogram), range from -2%
363 to +4% with the mean satellite-sonde offset 2.0% (sonde higher, **Table 3**, column 4). As
364 with many sonde-satellite comparisons, the ratios in 1998-2001 in the TOMS period are
365 mostly < 1.0; this changes to mostly > 1.0 in 2002, a value that applies for OMI comparisons
366 in the remainder of the first time-series and continues with the OMI and OMPS
367 comparisons with sonde and Dobson from late 2012 through 2016. These variations are
368 consistent with the statistics for satellite and Dobson coincidences at Irene (**Figure 5d**).

369 However, the Dobson/satellite differences are not large, similar to Natal (**Figure 5c**),
370 although at Irene, the ratio is slightly smaller for Dobson/TOMS than it is at Natal.

371 The Nairobi sondes (**Figure 4i**) are in excellent agreement with the three satellites
372 throughout the 1998-2016 period. The Nairobi histogram (right in **Figure 4i**) has the
373 highest absolute number of comparisons between sonde and satellites compared to the
374 other sites (scale up to 225). The peak is close to 1.0; the mean offset (**Table 3**) is -1.7%.
375 During the earliest part of the SHADOZ record, Nairobi (**Figure 4i**) sonde/satellite and
376 sonde/Dobson ratios are close to unity, which is higher than most of the other stations
377 examined so far. These ratios dip in 2002-2003, then increase in 2004 and even more in
378 the early OMI era. A preponderance of factors > 1.0 persists into mid-2010 when there is a
379 short gap. From late 2010 throughout mid-2014 the sonde ratio relative to OMI and OMPS
380 is close to unity. The Dobson/satellite statistics are summarized in **Figure 5e**, where the
381 ratios cluster near 1.0; there is less data than for the satellites because of Dobson gaps in
382 2000-2004 and 2012-2016. The lowest ratios in **Figure 5e** (blue shading) correspond to
383 the early OMI period (2005-2011) and are consistent with OMI total ozone being greater
384 than TOMS, for which the Dobson ratio peaks slightly higher than 1.0, like Natal and Irene
385 (**Figures 5 c,d**).

386 As described in **Section 2**, the ozone record at La Réunion (**Figure 4j**) represents
387 further reprocessing since Witte17a. Agreement among the sondes, TOMS and co-located
388 SAOZ is consistent from 1998-2004 with ratios ~0.95 or a mean sonde offset of -5%.
389 During the OMI period from 2005 to 2010, most of the sonde ratios increase to an average
390 ~1.0. In 2011-2012, most factors are > 1.0. After 2012 there is a slight drop-off, with a few
391 ratios below 0.9. These variations, taken across the 1998-2016 period, lead to a mean
392 offset of -0.9% for sonde-satellite (yellow in histogram, **Figure 4j**) and sonde-SAOZ
393 (hatched in histogram). In **Figure 5f** La Réunion SAOZ/satellite comparisons have a very
394 high sample number, with ratios for all three satellites peaking near 1.0.

395 For Kuala Lumpur (**Figure 4k**) from 1998 through 2012, fewer than 10 sonde/satellite
396 ratios were > 1.0, but in 2013, there is a jump to many more values > 1.0. This is followed
397 by a noisier record with factors both greater and less than 1.0 from late 2013 to early 2016.
398 If it is assumed that the Brewer is a stable reference, the satellite-Brewer total ozone
399 comparisons (**Figure 5g**) explain these changes. The Brewer/TOMS ratio indicates a

400 higher satellite reading in 1998-2004 than the Brewer so the sonde/satellite ratios (gray in
401 **Figure 4k**) are lower than for Brewer. For the OMI period (Brewer is lower than the
402 satellite, **Figure 5g**), higher sonde/satellite ratios are expected. They increase slightly from
403 2005 through 2009 (**Figure 4k**) and much more after the re-start of launches in 2012.
404 Most sonde/satellite ratios after 2012 are with OMPS ozone which the Brewer comparison
405 (**Figure 5g**) suggests measures more ozone than OMI so many ratios fall to < 1.0 (**Figure**
406 **4k**). Sonde offsets from the three satellites average -5.5% (yellow histogram, **Figure 4k**);
407 the Brewer histogram (hatched in **Figure 4k**) follows the satellite but with fewer samples.

408 At Hanoi (**Figure 4l**, note the late 2004 start) there have been two Brewer instruments
409 (**Table 1**). The first one spanned the beginning of the sondes in 2004 until 2012 but the
410 noisy data are so divergent from the satellites that we have not used them. Only
411 measurements from the second Brewer, with data from 2012 to 2014, are compared to the
412 sondes; we note that the Brewer/satellite ratios (**Figure 5h**) are much higher than OMI and
413 OMPS and are outside the guideline for ideal Brewer-satellite agreement (*Fioletov et al.*,
414 2008). The lower left panel in **Figure 4l**, as well as the small sample number in the
415 histogram (hatched, at right), show that sonde-Brewer coincidences are also infrequent.
416 Sonde-satellite offsets average -1.2%. The Hanoi sonde-satellite data across the OMI and
417 OMPS period until 2014 are fairly consistent (not surprising with similar statistics relative
418 to the Brewer, **Figure 5h**). From 2014 to 2016 the sonde/satellite ratios are nearly all
419 < 1.0 . The sonde-satellite histogram in **Figure 4l** has a long negative tail.

420 The SHADOZ data at Watukosek (**Figure 4m**) are compared to a Brewer at Bandung,
421 which is several hundred km to the west and at elevation 740 m (Watukosek is 50 m).
422 Watukosek is also frequently polluted near the surface by local pollution [T03; T12]. Many
423 Brewer readings have been removed in the comparisons, e.g., from 2009-2011, because
424 they diverged $> 10\%$ absolute from the satellite readings. However, those that remain give
425 ratios to OMI and OMPS that are well-centered about 1.0 (**Figure 5i**). The sonde/satellite
426 ratios (lower frame in **Figure 4m**) also average close to 1.0. There is a mean -1.3% offset in
427 the sonde-satellite histogram (yellow at right, **Figure 4m; Table 3**).

428 Fiji has no ground total ozone instrument (**Figure 4n**) and there are two year-plus
429 gaps in the measurement record. For the TOMS and early OMI period, from 1998-2005
430 when the first gap began, sonde/satellite ratios typically fall in the range 0.95-1.0. As for

431 most of the other SHADOZ stations, the sondes record more total ozone than the satellites
432 during the mid-OMI period, 2007-2013. In 2015 the ratios trend lower for both OMI and
433 OMPS, particularly in 2016. The histogram for the satellite comparisons (right, in yellow)
434 skews slightly negative, averaging 0.9% lower for the sondes (**Table 3**).

435 **3.1.2 Residual Discontinuities in Total-column Ozone Time-series**

436 The discussion of ratios in **Figure 4** shows that for nearly all of the SHADOZ stations
437 reprocessing has not completely resolved the systematic variability exhibited in the
438 original data [Witte17a]. In some cases, quite a bit of noise persists even though the mean
439 TCO is closer to both satellite total ozone and ground-based instruments and is presumed
440 to be more accurate than the original. **Section 3.1.1**, with satellite-ground-based-sonde
441 comparisons over three different satellites, suggests that variations among the satellite
442 sensors (discussed in Witte17b) and perhaps unevenly calibrated Dobsons or Brewers, is
443 one reason for persistent discontinuities in sonde ratios after reprocessing.

444 Several additional factors may also contribute. First, there is inherent uncertainty in
445 the ECC sonde measurement, which varies with altitude. This has been evaluated in
446 Witte17b for reprocessed SHADOZ ozone profiles and for the column amounts. Secondly,
447 the reprocessing prescribed in *Smit and ASOPOS* [2012] and *Deshler et al.* [2017] and
448 applied in Witte17a, Witte 17b and Sterling17 corrects only for variations in the ECC
449 sondes and their operating characteristics. The impact of the many ECC sonde-radiosonde
450 combinations (**Table 2**) used in SHADOZ has only partially been addressed. For example,
451 additional corrections were made by Witte17a and Sterling17 to compensate for what are
452 assumed to be incorrect pressure readings from iMet radiosondes [Stauffer *et al.*, 2014] at
453 five stations (**Table 2**). Vertical dashed lines in **Figures 4a,b,d, g** and **n** mark the first
454 deployment of the iMet radiosondes at each station. However, these first-order corrections
455 are not based on rigorous lab or field tests with ECC sondes. Looking at distinct changes in
456 the sonde ratios after 2013, their coincidence with the iMet changeover is only
457 straightforward for two datasets. One of those is for Fiji (**Figure 4n**). The other
458 discontinuity that coincides with iMet is at Ascension (**Figure 4g**), although the last part of
459 the LMS-SPC instrument combination (2009-2010) also displays sharply lower sonde
460 ratios relative to the record up to 2009. At Samoa, there is a sharp dropoff in ratios at the
461 start of the iMet period (2014 in **Figure 4a**) but there are clusters with values > 1.0 during

462 2015 and the latter part of 2016. At Hilo (**Figure 4b**) the falloff in the ratio lags the iMet
463 introduction by about a year; a similar delay is observed for Costa Rica (**Figure 4d**).

464 An additional factor in the residual discontinuity of sonde ratios could be the ECC
465 ozonesonde itself. For the six stations using the iMet radiosonde, the coupling is to
466 EnSci/DMT ECC ozonesondes. This instrument may have been inadvertently modified in
467 the 2011-2016 period as the manufacturer changed, first in 2012 when the original EnSci
468 Corporation became part of Droplet Measurement Technology (DMT), followed by a shift to
469 a new version of the EnSci Corporation in 2016. We tested this hypothesis for four stations
470 that use the EnSci sonde and where the sonde ratio dropped after 2013: Samoa, Hilo, Costa
471 Rica, Fiji. Several operating characteristics of the sondes, e.g., flow rate, background
472 current, total column ozone, were also examined as a function of the sonde date since 2006,
473 (using the 2Z serial number to track the ECC). Most parameters appeared to be
474 independent of time, except for a lower TCO amount at two stations (**Figure 6**). Total
475 ozone and the sonde/OMI (OMPS) ratio have dropped off ~15% at Costa Rica since late
476 2015 (**Figure 4d**); the relationship to serial number (**Figure 6, left**) suggests something
477 might have changed after No. 25000 but there is no clear cause when meta-data are
478 examined (this also agrees with findings by H. Vömel, *Private Communication*, 2017). At Fiji
479 (**Figure 6, right**) there have also been a few anomalously low TCO values in 2016, after the
480 2Z #25000 period. However, analysis of instruments used at Samoa and Hilo, where sonde
481 ratio falloffs after 2014 are observed (**Figures 4a,b**), does not show similar behavior. No
482 chamber tests have been carried out over the time of the evolving EnSci instrument. Field
483 tests with the EnSci sondes and the current suite of radiosondes (iMet, RS92, RS41, LMS)
484 need to be conducted. Moreover, the residual discontinuity in sonde ratios with this first
485 set of reprocessed SHADOZ data is a reminder that the current reprocessing guidelines do
486 not systematically account for radiosonde instrument changes at long-term stations.

487 **3.1.3 Summary of Reprocessed data and Satellite Total Ozone**

488 **Figure 7** summarizes mean total column ozone from TOMS-OMI-OMPS over each
489 SHADOZ station in black (with $\pm 1\sigma$ denoted by the bars). The mean sonde total column
490 ozone value is in red, with the $\pm 1\sigma$ range represented by the pink shading. **Table 3**
491 summarizes the corresponding mean sonde-satellite offsets over the 1998-2016 period,
492 except for Costa Rica and Hanoi, where the comparisons are for late 2004 or 2006 to 2016,

493 respectively. For all SHADOZ stations, reprocessing has improved the agreement of the
494 sondes with both the satellites and ground-instruments (Figure 11 in T12). With the
495 reprocessed data only two stations display a mean offset $> (\pm)2\%$ (**Figures 4, 7; Table 3**).
496 By contrast, in T07 (Figure 8), sondes for five of the ten stations were offset 5-10% from
497 OMI. Witte17a showed that the greatest improvements in satellite-sonde agreement are
498 for Hanoi and Watukosek (**Figures 4l,m**); this now applies to reprocessed Réunion, San
499 Cristóbal and Costa Rica data as well.

500 **3.2 Partial Column Ozone Comparisons, TTL Ozone Structure and the** 501 **Tropospheric Wave-One.**

502 In prior analyses of SHADOZ column ozone amounts, we computed ozone column
503 amounts within the stratosphere, troposphere and TTL, along with the structure of the
504 wave-one pattern in tropospheric ozone. Updates to these analyses appear in **Figures 8-**
505 **10**. In some of the station-to-station comparisons, as in T12, we focus on the 10 stations
506 designated as “tropical”. The latter sites are distinct from four stations that are subtropical
507 due to seasonally low tropopauses (*Baray et al., 1998; Diab et al., 2004; Ogino et al., 2013*):
508 Hilo, Irene, Réunion, Hanoi. The tropopause heights in km for the tropical sites are shown
509 in **Figure 3**, along with the TTL, here taken as 15-18.5 km or 130-70 hPa.

510 The stratospheric ozone column, depicted in **Figure 8a**, obtained by subtracting
511 tropospheric column ozone from total ozone (**Table 3**), includes the climatological add-on
512 amount above balloon burst. Except for Paramaribo, the other nine tropical stations
513 display a mean of 229 ± 3.9 DU. The relatively small 1σ values shown in **Figure 8a**
514 represent a significant improvement in data consistency for several stations compared to
515 earlier SHADOZ climatologies [T03; T07; T12]. For example, in the first compilation of
516 stratospheric ozone (Table 3, header 7, in T03) the Natal 1σ amount was 9% and in T12
517 (Table 4) it was 7.5%. This has been reduced to 5% after reprocessing (**Figure 8a**). There
518 are also absolute percentage changes of this order from T07 (Table 4) compared to the
519 reprocessed data for San Cristóbal, Ascension, Watukosek and Fiji. In summary,
520 reprocessing has reduced stratospheric column ozone variability (i.e, standard deviation)
521 to 5%. The TCO variability has improved accordingly. Inspection of the ranges and sonde
522 averages (pink edge and red circles in **Figure 7**) shows that they vary from 4-6%.

523 The TTL column for all 14 SHADOZ stations (**Figure 8b**) only shows two prominent
524 outliers, Hilo and Irene (numbered 2 and 8, respectively), not surprising because of their
525 subtropical character and expected higher ozone content. They share some of the highest
526 outliers as does the subtropical Réunion station (labeled 10 in **Figure 8b**). However,
527 Hanoi, also subtropical, does not stand out from the other tropical stations.

528 A major finding from the SHADOZ data, as described in *Thompson et al.* [2003b;
529 2001b] was the isolation of the “wave-one” pattern in total ozone first described by
530 *Fishman and Larsen* [1987] and *Shiotani* [1992] (cf Figure 4 of *Kim et al.*, 1996). For
531 tropical latitudes, the wave-one refers to 10-20 Dobson Units (DU) more column ozone
532 over the Atlantic and eastern Africa, a maximum relative to the central-western Pacific
533 ozone minimum. The SHADOZ observations from 1998-2000 [*Thompson et al.*, 2003b],
534 demonstrated that because there are no statistically significant differences among column-
535 integrated stratospheric ozone over the individual tropical stations (as in **Figure 8a**, **Table**
536 **3**), the additional ozone must reside in the troposphere. These findings apply to the
537 reprocessed data from 1998-2016 where detailed statistics, in the form of a box-and-
538 whisker plot (**Figure 8c**) for the ten tropical stations, are presented. Although **Figure 8c**
539 does not display station locations realistically, noting from **Figure 7** that the wave-one
540 maximum lies between Natal and Ascension, the wave magnitude can be approximated.
541 Based on the data in **Figure 8c** the mean tropospheric ozone maximum is ~38 DU. The
542 eastern Indian Ocean-to-Pacific minimum (**Figure 8c**) extends across four stations from
543 Kuala Lumpur to Samoa, where the range of tropospheric column ozone is 22-26 DU.
544 Taking the mean tropospheric column ozone of 24 DU to represent the zonal minimum, the
545 tropical wave magnitude is estimated as 14 DU. This is the same as estimated in T12.

546 A cross-section of mean TTL mixing ratios, from 15 to 18.5 km, based on 0.25 km
547 averages (**Figure 9a**), captures nearly uniform ozone mixing ratios above the nominal
548 tropopause (> 17 km) with distinct zonal variations below 16 km. Viewed on a seasonal
549 basis (**Figures 9b,c**) the zonal gradients are more pronounced. In March-April-May (MAM
550 in **Figure 9b**), a highly convective time of year at most tropical sites, the zonal gradients
551 across 15 km are greater than 50%. The same holds when subsidence and pollution
552 impacts in the UT are strongest between Paramaribo and Nairobi (eastern South America
553 to east Africa) in September-October-November (SON in **Figure 9c**).

554 Seasonal variations in tropospheric ozone, as in the TTL, cause the wave-one
555 magnitude to vary over the year (**Figure 10**). As in *Thompson et al.* [2003b] **Figure 10**
556 indicates that the wave-one is a minimum when most tropical stations are convectively
557 active (MAM). The maximum wave amplitude is observed in SON where there is greater
558 subsidence and pollution sources in the mid-troposphere from southern hemisphere
559 biomass fires [*Thompson et al.*, 1996; T12].

560 **3.3 Tropical Station-to-station Bias**

561 Our prior studies of station-to-station bias focused on the stratosphere because, as
562 **Figure 8a** implies, the total stratospheric ozone column for the tropical stations is uniform
563 within statistical significance. A mean tropical ozone profile from surface to 10 hPa has
564 been calculated from the ten most equatorward stations (seasonal means in **Figure 11**).
565 Note that in **Figure 11** the variability of two seasons, DJF (December-January-February)
566 and JJA (June-July-August), is greater than MAM and SON (larger 1σ standard deviations,
567 denoted by gray shading) in the troposphere and also near the stratospheric peak. The
568 high variability suggests that it may be difficult to compute reliable trends in the TTL
569 except in SON when ozone is a maximum and in MAM when ozone is a minimum [T03].

570 When the mean profile for each tropical station is referenced to an all-tropical profile
571 average based on **Figure 11**, the offsets illustrated in **Figure 12** are obtained. Results for
572 the three regions, eastern Indian Ocean to Pacific (labeled as W. Pacific in **Figure 12a**),
573 eastern Pacific (**Figure 12b**) and Atlantic plus Nairobi (**Figure 12c**) are shown separately.
574 It is assumed that above the region marked TTL, stratospheric ozone is zonally invariant
575 and that deviations from zero signify bias. All the offsets in **Figure 12** except for Fiji (blue
576 in **Figure 12a**) and Ascension near the TTL (red in **Figure 12c**) are 10% absolute or less.
577 The higher ozone over Fiji below 40 hPa likely owes to subtropical characteristics, perhaps
578 mixing of tropical and mid-latitude air, in the South Pacific Convergence Zone (the site is at
579 18°S , *Pickering et al.*, 2001). A nearly identical deviation from the other tropical stations
580 based on 1998-2009 Fiji data appears in Figure 13a of T12. Changes in Watukosek and
581 Kuala Lumpur offsets (**Figure 12a**) compared to T12 are mostly in the TTL. The three east
582 Pacific stations (Costa Rica grouped with the island sites, **Figure 12b**) are all close to the
583 mean and show almost no variation throughout the stratosphere. Compared to their T12
584 offsets, based on 1998-2009 data, Samoa and San Cristóbal in **Figure 12b** have increased

585 relative to the other stations. Samoa now has a slightly positive offset and San Cristóbal is
586 close to the zero line. These patterns for Samoa and San Cristóbal are also close to those
587 shown in T07 (Figure 5a) that were based on 1998-2004 observations.

588 In **Figure 12c** Nairobi is nearly on the zero line whereas it had a 5% high-bias in T12.
589 This is because reprocessing increases stratospheric ozone at many stations [Witte17a].
590 Paramaribo is consistently high (green in **Figure 12c**) as in T12. Natal is nearly unchanged
591 from T12 and Ascension is slightly more negative (red and blue, respectively, **Figure 12c**).
592

593 **4. Summary**

594 The first set of reprocessed data from 12 SHADOZ stations (1998-2016) and 2 stations
595 (2004-2016) with records covering at least a decade are evaluated in three ways. First,
596 total ozone from the sondes is compared to satellite overpass total ozone from the three
597 buv-type instrument series that cover the SHADOZ period, EP/TOMS up through 2004, and
598 the operational OMI (since September 2004) and OMPS, since February 2012. Total ozone
599 column coincident with the sondes are also compared to co-located ground-based
600 instruments at nine stations. The main findings are:

- 601 • Reprocessing leads to more consistent total ozone records within a given
602 station except for Paramaribo, which is currently being reprocessed again.
- 603 • Offsets between sonde total ozone and ozone from the satellite series are
604 greatly improved relative to T07 and T12. Two stations register mean absolute
605 sonde-satellite disagreements of 5% absolute; all others are within $\pm 2\%$. The
606 same applies to sonde TCO agreement with nine co-located ground-based
607 instruments.
- 608 • Although TCO from the sondes, satellites and ground-based instruments agree
609 better after reprocessing there is still unexplained noise in most time-series of
610 ratios and clear discontinuities when the sonde TCO is compared to the satellite
611 record. The two prominent features are: (1) the sonde/satellite TCO record
612 seems to vary among the satellites with TOMS v8 TCO running higher (lowest
613 sonde ratio) than the first 5-7 years of OMI (higher sonde ratio) before the
614 sonde ratio drops during the OMI-OMPS era. The pattern is confirmed through

615 comparison of the satellite and ground-based instrument TCO. (2) The second
616 discontinuity is observed after 2012-2014 at eight stations with the sonde ratio
617 dropping relative to OMI, OMPS and, where applicable, the local ground-based
618 instrument. This suggests that something is shifting in the sondes. Radiosonde
619 changes appear to play a role at several stations and changes in the ECC sonde
620 can be detected at Costa Rica and Fiji. However, the statistics for the post-2012
621 drop in sonde ratio are limited compared to a 19-year record for most SHADOZ
622 stations. These patterns are being investigated further. Possible ECC sonde
623 issues will be addressed in JOSIE-type chamber tests in the near future.

624 The second analysis of the reprocessed data examined three partial column amounts
625 for ten tropical stations, defined as having at latitude < 19 degrees: stratospheric ozone,
626 tropospheric ozone, ozone in the tropical tropopause layer (TTL). As in our prior
627 comparisons [T03; T07; T12] the stratospheric column was zonally invariant except for
628 slightly elevated amounts over Paramaribo. In addition:

- 629 • The TTL column amount is also invariant across the ten stations (9 ± 1 DU) and two
630 subtropical stations, Réunion and Hanoi, display nearly the same value. However,
631 there is considerable zonal structure below 17 km at all times of year, with strong
632 vertical gradients over the western Pacific and eastern Indian Ocean. These features
633 are not well-resolved by profiling satellites which argues for caution in trends based
634 on satellite data below 70 hPa.
- 635 • The tropospheric wave-one feature first characterized with SHADOZ data from nine
636 stations [*Thompson et al., 2003b*] is better delineated with the addition of Costa
637 Rican data. The mean amplitude of the wave is 14 DU.
- 638 • Reprocessing has reduced the standard deviation of stratospheric and total column
639 ozone at SHADOZ stations to 5%.

640 Third, using mean profiles, we examined mid-stratospheric bias given that the
641 stratospheric column appears to be zonally invariant among the 10 tropical sites. At all but
642 two stations the bias above 70 hPa has improved relative to the T07 and T12 analyses; the
643 mean for all stations less than 10% absolute. This demonstrates that key elements in
644 reprocessing procedures, using appropriate pump corrections, applying transfer functions,

645 screening for anomalous background currents, and, in general, applying corrections that
646 account for known biases in the ozonesonde system, indeed homogenize SHADOZ data.
647 The results underscore the need for complete meta-data in archived sonde records.

648 Satellite-based tropospheric ozone products and models suitable for exploring
649 complex variability in the tropics are still in development. Given the improvements
650 quantified in this study, we expect reprocessed SHADOZ data to become a standard
651 reference for evaluating new satellites, emerging tropospheric ozone products, assessment
652 model simulations and for detecting satellite drift. In addition, the seasonal and
653 longitudinal variations in TTL ozone structure observed in SHADOZ data, as well as our
654 classification of tropospheric profiles by self-organizing maps [Jensen *et al.* 2012; Stauffer *et*
655 *al.*, 2016] suggest that more attention be given to tropical satellite retrievals below the
656 stratosphere. In the TTL critical interactions take place among ozone, water vapor,
657 temperature and dynamics; in the free troposphere ozone mediation of OH determines
658 atmospheric lifetimes for myriad species.

659
660 **Acknowledgments.** SHADOZ is sponsored by the Upper Atmosphere Research Program of NASA (special
661 thanks to K. W. Jucks) and Aura Validation. Support from NOAA's Global Monitoring Division and many other
662 international agencies, in every country where SHADOZ operates, from the Netherlands and Switzerland in
663 Europe as well as Japan, is gratefully acknowledged. All SHADOZ operators and data managers are thanked
664 for their dedication to SHADOZ over the past 20 years. We also appreciate helpful comments of three
665 reviewers.

666

667 **Acronyms**

668 BESOS = Balloon Experiment on Standards for Ozone Sondes
669 BUV = Back-scattered Ultraviolet
670 CPT = Cold-point Tropopause
671 DJF = December-January-February
672 DU = Dobson Unit; 1 DU=2.69 x10¹⁶ molec cm⁻²
673 ECC = Electrochemical Concentration Cell
674 ENSO = El Niño Southern Oscillation
675 FT = Free Troposphere
676 GOME = Global Ozone Monitoring Experiment (ERS-2 GOME, 1995-2011; GOME II, 2003-, 2012-)
677 IASI = Infrared Atmospheric Sounder Instrument
678 IO3C = International Ozone Commission
679 IGACO = Integrated Global Atmospheric Chemistry Observations
680 IPCC = Intergovernmental Panel for Climate Change
681 JJA = June-July-August
682 JOSIE = Jülich Ozonesonde Intercomparison Experiment; (<http://www.fz-juelich.de/icg/icg-2/josie>)

683 LRT = Lapse-Rate Tropopause
 684 LS = Lower Stratosphere
 685 MAM = March-April-May
 686 MLS = Microwave Limb Sounder (on UARS, 1991-2005; on Aura, 2004-)
 687 NASA = National Aeronautics and Space Administration
 688 NDACC = Network for Detection of Atmospheric Composition Change (<http://www.ndacc.org>)
 689 NOAA = National Oceanic and Atmospheric Administration
 690 NPP = National Polar-Orbiting Partnership
 691 OMI = Ozone Monitoring Instrument (on Aura, 2004-)
 692 OMPS = Ozone Mapper Profiler Suite (on S-NPP, October 2011-)
 693 PTU = Pressure-Temperature-Humidity (data from radiosonde)
 694 QBO = Quasi-biennial Oscillation
 695 SAOZ = System d'Analyse par Observation Zenitale (<http://gosc.org/gcos/SAOZ-prog-overview.html>)
 696 SCIAMACHY = Scanning Imaging Absorption SpectroMeter for Atmospheric ChartographY (2002-2012)
 697 SHADOZ = Southern Hemisphere Additional Ozonesondes; (<http://tropo.gsfc.nasa.gov/shadoz>)
 698 TC⁴ = Tropical Composition, Clouds and Climate Coupling; (<http://www.espo.nasa.gov/tc4/>) (2007)
 699 TOMS = Total Ozone Mapping Spectrometer (in SHADOZ era, Earth-Probe/TOMS, 1996-2005)
 700 TTL = Tropical Tropopause Layer
 701 UT/LS = Upper Troposphere/Lower Stratosphere
 702 WMO = World Meteorological Organization
 703 WOUDC = World Ozone and Ultraviolet Data Centre; (<http://woudc.org>)
 704

705 REFERENCES

- 706 Baray, J. L., G. Ancellet, F. G. Taupin, M. Bessafi, S. Baldy, and P. Keckhut (1998), Subtropical
 707 tropopause break as a possible stratospheric source of ozone in the tropical troposphere, *J.*
 708 *Atmos. Sol.-Terr. Phys.*, **1**(60), 27–36, doi: [10.1016/S1364-6826\(97\)00116-8](https://doi.org/10.1016/S1364-6826(97)00116-8)
 709 Bethan, S., Vaughan, G. and Reid, S. J. (1996), A comparison of ozone and thermal tropopause
 710 heights and the impact of tropopause definition on quantifying the ozone content of the
 711 troposphere. *Q. J. R. Meteorol. Soc.*, **122**: 929–944. doi:10.1002/qj.49712253207.
 712 Deshler, T., et al. (2008), Atmospheric comparison of electrochemical cell ozonesondes from
 713 different manufacturers, and with different cathode solution strengths: The Balloon Experiment
 714 on Standards for Ozonesondes, *J. Geophys. Res.*, **113**, D04307, doi:10.1029/2007JD008975.
 715 Deshler, T., Stübi, R., Schmidlin, F. J., Mercer, J. L., Smit, H. G. J., Johnson, B. J., Kivi, R., and Nardi, B.
 716 (2017), Methods to homogenize electrochemical concentration cell (ECC) ozonesonde
 717 measurements across changes in sensing solution concentration or ozonesonde manufacturer,
 718 *Atmos. Meas. Tech.*, **10**, 2021-2043, doi:10.5194/amt-10-2021-2017.
 719 Diab, R. D., A. M. Thompson, K. Mari, L. Ramsay, and G. J. R. Coetzee (2004), Tropospheric ozone
 720 climatology over Irene, South Africa from 1990-1994 and 1998-2002, *J. Geophys. Res.*, **109**, D20,
 721 D20301, doi:10.1029/2004JD004293.
 722 Eyring, V., et al. (2005) A strategy for process-oriented validation of coupled chemistry-climate
 723 models, *Bull. Am. Meteor. Soc.*, **86**, 1117-1133, doi:[10.1175/BAMS-86-8-1117](https://doi.org/10.1175/BAMS-86-8-1117)
 724 Fioletov, V. E., et al. (2008), Performance of the ground-based total ozone network assessed using
 725 satellite data, *J. Geophys. Res.*, **113**, D14313, doi:10.1029/2008JD009809.
 726 Fishman, J., and J. C. Larsen (1987), Distribution of total ozone and stratospheric ozone in the
 727 tropics - Implications for the distribution of tropospheric ozone, *J. Geophys. Res.*, **92**, 6627-6634.
 728 Folkins, I., C. Braun, A. M. Thompson, and J. C. Witte, (2002), Tropical ozone as in indicator of deep
 729 convective outflow, *J. Geophys. Res.*, **107**, D13, doi:10.1029/2001JD001178.
 730 Fortuin, J. P. F., C. R. Becker, M. Fujiwara, F. Immeler, H. M. Kelder, M. P. Scheele, O. Schrems, and G. H.
 731 L. Verver (2007), Origin and transport of tropical cirrus clouds observed over Paramaribo,
 732 Suriname (5.8°N, 55.2°W), *J. Geophys. Res.*, **112**, D09107, doi:10.1029/2005JD006420.

733 Fueglistaler, S., A. E. Dessler, T. Dunkerton, I. Folkins, Q. Fu and P. W. Mote (2009), The tropical
734 tropopause layer, *Rev. Geophys.*, **47**, RG1004, doi:10.1029/2008RG000267.

735 Fujiwara, M., F. Hasebe, M. Shiotani, N. Nishi, H. Vömel, and S. J. Oltmans (2001), Water vapor
736 control at the tropopause by equatorial Kelvin waves observed over the Galápagos, *J. Geophys.*
737 *Res.*, **28**, 3143-3146, doi:10.1029/2001GL013310.

738 Gebhardt, C., A. Rozanov, R. Hommel, M. Weber, J. P. Burrows, D. Degenstein, L. Froidevaux, and A.
739 M. Thompson (2014), Stratospheric ozone trends and variability as seen by SCIAMACHY from
740 2002-2011, *Atmos. Chem. Phys.*, **14**, 831-846, 2014. doi: 10.5194/acp-14-831/2014.

741 Gettelman, A., and P. M. DeF. Forster (2002), A climatology of the tropical tropopause layer, *J.*
742 *Meteor. Soc. Japan*, **80**, No. 4B, 911-924, doi:10.2151/jmsj.80.911.

743 Hubert, D., et al. (2016), Ground-based assessment of the bias and long-term stability of 14 limb and
744 occultation ozone profile data records, *Atmos. Meas. Tech.*, **9**, 2497-2534, doi:10.5194/amt-9-
745 2497-2016.

746 Heue, K.-P., M. Coldewey-Egbers, A. Delcloo, C. Lerot, D. Loyola, P. Valks, and M. van Roozendael
747 (2016), Trends of tropical tropospheric ozone from 20 years of European satellite
748 measurements and perspectives for the Sentinel-5 Precursor, *Atmos. Meas. Tech.*, **9**, 5037-5051,
749 doi:10.5194/amt-9-5037-2016.

750 Intergovernmental Panel for Climate Change (2007) Climate Change 2007: The physical science
751 basis: Contribution of Working Group I to the Fourth Assessment Report of the
752 Intergovernmental Panel on Climate Change, S. Solomon, D. Qin, M. Manning, Z. Chen, M.
753 Marquis, K. B. Averyt, M. Tignor, H. L. Miller, Editors, Cambridge Univ Press, Cambridge, UK.

754 Jensen, A. A., A. M. Thompson, and F. J. Schmidlin (2012), Classification of Ascension Island and
755 Natal ozonesondes using self-organizing maps, *J. Geophys. Res.*, **117**, D04302,
756 doi:10.1029/2011JD016573.

757 Johnson, B. J., S. J. Oltmans, H. Voemel, H. G. J. Smit, T. Deshler, and C. Kroeger (2002), ECC
758 ozonesonde pump efficiency measurements and tests on the sensitivity to ozone of buffered and
759 unbuffered ECC sensor cathode solutions, *J. Geophys. Res.*, **107**, D19, 4393,
760 doi:10.1029/2001JD000557.

761 Kaminski, J., et al. (2008), GEM-AQ, an online global multiscale chemical weather modeling system:
762 model description and evaluation of gas phase chemistry, *Atmos. Chem. Phys.* **8**, 3255-3281.

763 Kim, J-H., R. D. Hudson, and A. M. Thompson (1996), A new method of deriving time-averaged
764 tropospheric column ozone over the tropics using TOMS radiances: Intercomparison and
765 analysis. *J. Geophys. Res.*, **101**, 24317-24330, doi:10.1029/96JD01223.

766 Komhyr, W.D. (1969), Electrochemical concentration cells for gas analysis, *Ann. Geoph.*, **25**, 203-210.

767 Komhyr, W. D. (1986), Operations handbook - Ozone measurements to 40 km altitude with model
768 4A-ECC-ozone sondes, NOAA Techn. Memorandum, ERL-ARL-149.

769 Komhyr, W. D., R. A. Barnes, G. B. Brothers, J. A. Lathrop, and D. P. Opperman (1995),
770 Electrochemical concentration cell ozonesonde performance evaluation during STOIC 1989, *J.*
771 *Geophys. Res.*, **100**, 9231-9244, doi:10.1029/94JD02175.

772 Labow, G. J., J. R. Ziemke, R. D. McPeters, D. P. Haffner, and P. K. Bhartia (2015) A total ozone-
773 dependent ozone profile climatology based on ozonesondes and Aura MLS data, *J. Geophys. Res.*
774 *Atmos.*, **120**, 2537-2545, doi:10.1002/2014JD022634.

775 Liu, G., J.J. Liu, D.W. Tarasick, V.E. Fioletov, J.J. Jin, O. Moeni, X. Liu, C.E. Sioris and M. Osman (2013), A
776 global tropospheric ozone climatology from trajectory-mapped ozone soundings, *Atmos. Chem.*
777 *Phys.* **13**, 10659-10675, doi:10.5194/acp-13-10659-2013.

778 Liu, J., D.W. Tarasick, V.E. Fioletov, C. McLinden T. Zhao, S. Gong, C. Sioris, J. Jin, G. Liu, and O. Moeini
779 (2013), A global ozone climatology from ozone soundings via trajectory mapping: A
780 Stratospheric Perspective, *Atmos. Chem. Phys.*, **13**, 11441- 11464, doi:10.5194/acp-13-11441-
781 2013.

782 Martin, R.V., et al. (2002), Interpretation of TOMS observations of tropical tropospheric ozone with
783 a global model and in situ observations. *J. Geophys. Res.*, **107**(D18), 4351,
784 doi:10.1029/2001JD001480.

785 McPeters, R. D., and G. J. Labow (2012) Climatology 2011: An MLS and sonde derived ozone
786 climatology for satellite retrieval algorithms, *J. Geophys. Res.*, **117**, D10303, doi:
787 10.1029/2011JD017006.

788 McPeters, R. D., G. J. Labow, and J. A. Logan (2007), Ozone climatological profiles for satellite
789 retrieval algorithms, *J. Geophys. Res.*, **112**, D05308, doi:10.1029/2005JD006823.

790 Newton, R., G. Vaughan, H. M. A. Ricketts, L. L. Pan, A. J. Weinheimer, and C. Chemel (2016),
791 Ozonesonde profiles from the West Pacific Warm Pool: Measurements and validation. *Atmos.*
792 *Chem, Phys.*, **16**, 619-634, doi:10.5194/acp-16-619-2016.

793 Ogino, S.-Y., M. Fujiwara, M. Shiotani, F. Hasebe, J. Matsumoto, T. H. T. Hoang, and T. T. T. Nguyen
794 (2013), Ozone variations over the northern subtropical region revealed by ozonesonde
795 observations in Hanoi, *J. Geophys. Res. Atmos.* **118**, 3245–3257, doi:10.1002/jgrd.50348.

796 Oltmans, S. J., et al. (2004), Tropospheric ozone over the North Pacific from ozonesonde
797 observations, *J. Geophys. Res.*, **109**, D15S01, doi:10.1029/2003JD003466.

798 Peters, W., M. C. Krol, J. P. F. Fortuin, H. M. Kelder, C. R. Becker, A. M. Thompson, J. Lelieveld, and P. J.
799 Crutzen (2004), Tropospheric ozone over a tropical Atlantic station in the Northern
800 Hemisphere: Paramaribo, Surinam (6N, 55W), *Tellus B*, **56**, 21-34, doi:10.1111/j.1600-
801 0889.2004.00083.x

802 Pickering, K. E., et al. (2001), Trace gas transport and scavenging in PEM-Tropics B South Pacific
803 Convergence Zone convection, *J. Geophys. Res.*, **106**(D23), 32591–32607,
804 doi:[10.1029/2001JD000328](https://doi.org/10.1029/2001JD000328)..

805 Proffitt, M. H., and R. J. McLaughlin (1983), Fast response dual-beam UV-absorption photometer
806 suitable for use on stratospheric balloons, *Rev. Sci. Instrum.*, **54**, 1719-1728, doi:
807 <http://dx.doi.org/10.1063/1.1137316>.

808 Randel, W. J., and A. M. Thompson (2011), Interannual variability and trends in tropical ozone
809 derived from SHADOZ ozonesondes and SAGE II satellite data, *J. Geophys. Res.*, **116**, D07303,
810 doi:10.1029/2010JD015195.

811 Sauvage, B., V. Thouret, A. M. Thompson, J. C. Witte, J.-P. Cammas, P. Nédélec, and G. Athier (2006),
812 Enhanced view of the “tropical Atlantic ozone paradox” and “zonal wave one” from the in situ
813 MOZAIC and SHADOZ data, *J. Geophys. Res.*, **111**, D01301, doi:10.1029/2005JD006241.

814 Selkirk, H. B., H. Vömel, J. M. Valverde Canossa, L. Pfister, J. A. Diaz, W. Fernández, J. Amador, W.
815 Stolz, and G. S. Peng (2010), Detailed structure of the tropical upper troposphere and lower
816 stratosphere as revealed by balloon sonde observations of water vapor, ozone, temperature, and
817 winds during the NASA TCSP and TC4 campaigns, *J. Geophys. Res.*, **115**, D00J19,
818 doi:10.1029/2009JD013209.

819 Shiotani, M. (1992), Annual, Quasi-Biennial, and El Niño-Southern Oscillation (ENSO) Time-Scale
820 Variations in Equatorial Total Ozone, *J. Geophys. Res.*, **97**(D7), 7625–7633,
821 doi:10.1029/92JD00530.

822 Sivakumar, V., H. Bencherif, N. Begue, A. M. Thompson (2011), Tropopause characteristics and
823 variability from 11-year SHADOZ observations in southern tropics and subtropics, *J. Appl.*
824 *Meteor. Clim.*, **50**, 1403-1416, doi:[10.1175/2011JAMC2453.1](https://doi.org/10.1175/2011JAMC2453.1)

825 Smit H.G.J and D. Kley (1998), JOSIE: The 1996 WMO International intercomparison of ozonesondes
826 under quasi flight conditions in the environmental simulation chamber at Jülich, WMO/IGAC-
827 Report, WMO Global Atmosphere Watch report series, No. 130 (Technical Document No. 926).
828 World Meteorological Organization, Geneva.

829 Smit, H. G. J., and W. Straeter (2004), JOSIE-1998, Performance of ECC Ozone Sondes of SPC-6A and
830 ENSCI-Z Type, WMO Global Atmosphere Watch report series, No. 157 (Technical Document No.
831 1218), World Meteorological Organization, Geneva.

832 Smit, H. G. J., et al. (2007), Assessment of the performance of ECC-ozonesondes under quasi-flight
833 conditions in the environmental simulation chamber: Insights from the Juelich Ozone Sonde
834 Intercomparison Experiment (JOSIE), *J. Geophys. Res.*, **112**, D19306,
835 doi:10.1029/2006JD007308.

836 Smit, H. G. J., and the Panel for the Assessment of Standard Operating Procedures for Ozonesondes
837 (ASOPOS) (2012), Guidelines for homogenization of ozonesonde data, SI2N/O3S-DQA activity as
838 part of “Past changes in the vertical distribution of ozone assessment”, available at: [http://www-
839 das.uwyo.edu/%7Edeshler/NDACC_O3Sondes/O3s_DQA/O3S-DQA-
840 Guidelines%20Homogenization-V2-19November2012.pdf](http://www-das.uwyo.edu/%7Edeshler/NDACC_O3Sondes/O3s_DQA/O3S-DQA-Guidelines%20Homogenization-V2-19November2012.pdf).

841 Smit, H. G. J. and the Panel for the Assessment of Standard Operating Procedures for Ozonesondes
842 (ASOPOS) (2014), Quality assurance and quality control for ozonesonde measurements in GAW,
843 World Meteorological Organization, GAW Report #201, available at:
844 http://www.wmo.int/pages/prog/arep/gaw/documents/FINAL_GAW_201_Oct_2014.pdf.

845 Stauffer, R. M., G. A. Morris. A., M. Thompson, E. Joseph, G. J. R. Coetzee, and N. R. Nalli (2014),
846 Propagation of radiosonde pressure sensor errors to ozonesonde measurements, *Atmos. Meas.
847 Tech.*, **7**, 65-79. doi:10.5194/amt-7-65-2014.

848 Stauffer, R. M., A. M. Thompson, and G. S. Young (2016), Free tropospheric ozonesonde profiles at
849 long-term U.S. monitoring sites: 1. A climatology based on self-organizing maps, *J. Geophys. Res.*,
850 **121**, doi:10.1002/2015JD023641.

851 Stevenson, D. S., et al. (2006), Multimodel ensemble simulations of present-day and near-
852 future tropospheric ozone, *J. Geophys. Res.*, **111**, D08301, doi:10.1029/2006JD006338.

853 Takashima, H., and M. Shiotani (2007), Ozone variation in the tropical tropopause layer as
854 seen from ozonesonde data, *J. Geophys. Res.*, **112**, D11123, doi:10.1029/2006JD008322.

855 Tarasick, D.W., J. J. Jin, V. E. Fioletov, G. Liu, A. M. Thompson, S. J. Oltmans, J. Liu, C. E. Sioris,
856 X. Liu, O. R. Cooper, T. Dann and V. Thouret (2010), High-resolution tropospheric ozone
857 fields for INTEX and ARCTAS from IONS ozonesondes, *J. Geophys. Res.*, **115**, D20301,
858 doi:10.1029/2009JD012918.

859 Tarasick, D. W., J. Davies, H. G. J. Smit, and S. J. Oltmans (2016), A re-evaluated Canadian
860 ozonesonde record: measurements of the vertical distribution of ozone over Canada
861 from 1966 to 2013, *Atmos. Meas. Tech.*, **9**, 195-214, doi:10.5194/amt-9-195-2016.

862 Thompson, A. M., et al. (1996), Where did tropospheric ozone over southern Africa and the
863 tropical Atlantic come from in October 1992? Insights from TOMS, GTE TRACE A, and
864 SAFARI 1992, *J. Geophys. Res.*, **101**(D19), 24,251–24,278, doi:10.1029/96JD01463.

865 Thompson, A. M., B. G. Doddridge, J. C. Witte, R. D. Hudson, W. T. Luke, J. E. Johnson, B. J.
866 Johnson, S. J. Oltmans, and R. Weller (2000), A tropical Atlantic Paradox: Shipboard and
867 satellite views of a tropospheric ozone maximum and wave-one in January–February
868 1999, *Geophys. Res. Lett.*, **27**(20), 3317–3320, doi:10.1029/1999GL011273.

869 Thompson, A. M., et al. (2003a), Southern Hemisphere Additional Ozonesondes (SHADOZ)
870 1998–2000 tropical ozone climatology 1. Comparison with Total Ozone Mapping
871 Spectrometer (TOMS) and ground-based measurements, *J. Geophys. Res.*, **108**, 8238,
872 doi:10.1029/2001JD000967.

873 Thompson, A. M., et al. (2003b), Southern Hemisphere Additional Ozonesondes (SHADOZ)
874 1998–2000 tropical ozone climatology 2. Tropospheric variability and the zonal wave-
875 one, *J. Geophys. Res.*, **108**, 8241, doi:10.1029/2002JD002241.

876 Thompson, A. M., J. C. Witte, H. G. J. Smit, S. J. Oltmans, B. J. Johnson, V. W. J. H. Kirchhoff, and
877 F. J. Schmidlin (2007), Southern Hemisphere Additional Ozonesondes (SHADOZ) 1998–
878 2004 tropical ozone climatology: 3. Instrumentation, station-to-station variability, and
879 evaluation with simulated flight profiles, *J. Geophys. Res.*, **112**, D03304,
880 doi:10.1029/2005JD007042.

881 Thompson, A. M., et al. (2010), Convective and wave signatures in ozone profiles over the
882 equatorial Americas: Views from TC4 2007 and SHADOZ, *J. Geophys. Res.*, **115**, D00J23,
883 doi:10.1029/2009JD012909.

884 Thompson, A. M., A. L. Allen, S. Lee, S. K. Miller, and J. C. Witte (2011a), Gravity and Rossby
885 wave signatures in the tropical troposphere and lower stratosphere based on Southern
886 Hemisphere Additional Ozonesondes (SHADOZ), 1998–2007, *J. Geophys. Res.*, **116**,
887 D05302, doi:10.1029/2009JD013429.

888 Thompson, A. M., S. J. Oltmans, D. W. Tarasick, P. Von der Gathen, H. G. J. Smit, J. C. Witte,
889 (2011b), Strategic ozone sounding networks: Review of design and accomplishments,
890 *Atmos. Environ.*, **45**, 2145-2163, doi:10.1016/j.atmosenv.2010.05.002.

891 Thompson, A. M., et al. (2012) Southern Hemisphere Additional Ozonesondes (SHADOZ)
892 tropical ozone climatology: Tropospheric and tropical tropopause layer (TTL) profiles
893 with comparisons to OMI-based ozone products. *J. Geophys. Res.*, **117**, D23301, doi:
894 10.1029/2010JD016911.

895 Thompson, A. M., N. V. Balashov, J. C. Witte, G. J. R. Coetzee, V. Thouret, F. Posny (2014),
896 Tropospheric ozone increases in the southern African region: Bellwether for rapid
897 growth in southern hemisphere pollution? *Atmos. Chem. Phys.*, **14**, 9855-9869,
898 doi:10.5194/acp-14-9855-2014

899 Thouret, V., et al. (2009), An overview of two years of ozone soundings over Cotonou as part
900 of AMMA. *Atmos. Chem. Phys.*, **9**, 6157-6174.

901 Tilmes, S. et al. (2012) Technical Note: Ozonesonde climatology between 1995 and 2011:
902 description, evaluation and applications, *Atmos. Chem. Phys.*, **12**, 7475-7497,
903 doi:10.5194/acp-12-7475-2012.

904 Van Malderen, R., M. A. F. Allaart, H. De Backer, H. G. J. Smit, and D. De Muer (2016) On
905 instrumental errors and related correction strategies of ozonesondes: possible effect on
906 calculated ozone trends for the nearby sites Uccle and De Bilt, *Atmos. Meas. Tech.*, **9**,
907 3793-3816, doi:10.5194/amt-9-3793-2016.

908 Vömel, H., S. J. Oltmans, B. J. Johnson, F. Hasebe, M. Shiotani, M. Fujiwara, N. Nishi, M. Agama,
909 J. Cornejo, F. Paredes, and H. Enriquez (2002), Balloon-borne observations of water
910 vapor and ozone in the tropical upper troposphere and lower stratosphere, *J. Geophys.*
911 *Res.*, 107(D14), doi:10.1029/2001JD000707.

912 Witte, J. C., et al. (2017a), First reprocessing of Southern Hemisphere ADDitional Ozone-
913 sondes (SHADOZ) profile records (1998-2015): 1. Methodology and evaluation, *J.*
914 *Geophys. Res. Atmos.*, **122**, doi:10.1002/2016JD026403.

915 WMO (World Meteorological Organization) (2007), *Scientific Assessment of Ozone Depletion:*
916 *2006*, Global Ozone Research and Monitoring Project - Report No. 50, 572pp., Geneva.

917 WMO (World Meteorological Organization) (2011), *Scientific Assessment of Ozone Depletion:*
918 *2010*, Global Ozone Research and Monitoring Project - Report No. 52, 516pp., Geneva.

919 WMO (World Meteorological Organization) (2014), *Scientific Assessment of Ozone Depletion:*
920 *2014*, Global Ozone Research and Monitoring Project - Report No. 55, 416pp., Geneva.

921 Yonemura, S., H. Tsuruta, S. Kawashima, S. Sudo, L. C. Peng, L. S. Fook, Z. Johar, and M. Hayashi
922 (2002), Tropospheric ozone climatology over Peninsular Malaysia from 1992 to 1999, *J. Geophys.*
923 *Res.*, 107, 4229, doi:10.1029/2001JD000993.

924

925 **FIGURE CAPTIONS 3 Oct**

926

927 **Figure 1** Map of SHADOZ stations for which reprocessed data are analyzed in this paper,
928 within the years 1998-2016. Period of operations and sample numbers are in **Table 1**.
929 Technical details of the reprocessing appear in Witte17a and Sterling17. Details for
930 SHADOZ sondes used at each site during 1998-2004, the Earth-Probe/TOMS period, appear
931 in *Thompson et al.* [2003a, 2007].

932

933 **Figure 2** Timeline of satellite ozone instruments that have used SHADOZ for validation.
934 Beyond 2017, expected lifetime for operational sensors is indicated with satellites
935 scheduled for launch by US and international partnerships in red.

936

937 **Figure 3** Box-and-whisker plot of tropopause heights are shown for the 10 SHADOZ
938 stations within ± 19 degrees of the equator, designated as “tropical”. Yellow boxes show the
939 interquartile of the 25th, median, and 75th percentiles. Outliers are displayed as blue circles.
940 The TTL region is bounded by the dashed lines.

941

942 **Figure 4** Time-series of TOMS-OMI-OMPS overpass total column ozone (O_3 , gray-black-
943 silver lines, respectively) with ozonesonde total column O_3 (red circles) values that reached
944 10 hPa. *McPeters and Labow* (2012) O_3 climatology is added from 10 hPa to the top-of-the-
945 atmosphere to yield sonde total column amounts. After February 2012 OMI and OMPS
946 operated simultaneously. Where available, total column O_3 from co-located Dobson, Brewer
947 or SAOZ instruments (blue cross) is given. The lower panel includes sonde/satellite and
948 sonde/ground instrument ratios. Here too, after February 2012, sonde/satellite ratios
949 include both OMI (black circles) and OMPS (silver circles). Histograms of the percent
950 difference with respect to sondes are also given for each station (yellow). Where available,
951 the percent difference is also shown between the sondes and ground-based total column O_3
952 (blue hashed). (a) American Samoa; (b) Hilo, Hawaii; (c) San Cristóbal; (d) Costa Rica; (e)
953 Paramaribo; (f) Natal; (g) Ascension; (h) Irene; (i) Nairobi; (j) Réunion; (k) Kuala Lumpur;
954 Hanoi; (m) Watukosek; (n) Fiji. Satellite overpasses are filtered for reflectivity greater
955 than 0.6 and distance from the station location greater than 200 km.

956

957 **Figure 5** Histograms of the ratio of total column O_3 from the ground-based instruments at
958 nine stations and coincident satellite measurements from TOMS (yellow-solid), OMI (blue-
959 hashed), OMPS (green-hashed). (a) American Samoa; (b) Paramaribo; (c) Natal; (d) Irene;
960 (e) Nairobi; (f) Réunion; (g) Kuala Lumpur; (h) Hanoi; (i) Watukosek.

961

962 **Figure 6** ECC sensor serial number (ENSCI 2Z type divided by 1000) versus total column O_3
963 at Costa Rica (left panel) and Fiji (right panel) since 2005.

964

965 **Figure 7** Longitudinal cross-section of 1998-2016 reprocessed sonde total column O_3 (red
966 circles with $\pm 1\sigma$ light red shading) and the collective mean TOMS-OMI-OMPS overpass
967 columns (black with $\pm 1\sigma$ black bars). Comparison of total column amounts from the
968 satellites and reprocessed sonde O_3 , on average, appear in **Table 3**, column 4.

969

970 **Figure 8** For the 10 tropical SHADOZ stations within ± 19 degrees of the equator, box-and-
971 whisker plots of (a) integrated column amounts of stratospheric O_3 (in DU) based on 1998-
972 2016 reprocessed data, (b) TTL column amounts from 15-18.5 km (130-70 hPa) for all
973 SHADOZ stations, and (c) tropospheric column amounts integrated from the surface to the

974 tropopause showing the characteristic wave-one pattern. Yellow boxes denote the
975 interquartile ranges.

976

977 **Figure 9** (a) Longitudinal cross-section of O_3 mixing ratios (units of ppm), computed from
978 0.25 km averages of 1998-2016 reprocessed data, for the 10 tropical stations, labeled by
979 country, within the TTL region. (b, c) same as (a) except for seasons MAM and SON,
980 respectively, and labeled by station. Labeling by Comparing to Figure 8b, where the column
981 amounts are statistically identical, distinctions in O_3 structure in the cross-section are
982 pronounced.

983

984 **Figure 10** Same as **Figure 9**, except contours of O_3 mixing ratio in the troposphere up to
985 the lower region of the TTL where the wave-one pattern appears, as in T03 and T12. Four
986 seasons illustrated: (a) SON; (b) DJF; (c) MAM; (d) JJA.

987

988 **Figure 11** 1998-2016 seasonally averaged O_3 partial pressure profiles (units of nbar) for
989 the ten reprocessed tropical stations. (a) SON; (b) DJF; (c) MAM; (d) JJA.

990

991 **Figure 12** Deviations from the 1998-2016 mean climatological profile from 100 to 10 hPa.
992 TTL upper boundary is marked by the dashed line. Above the TTL, in the stratosphere,
993 station offset differences are more likely to indicate bias. (a) western Pacific and eastern
994 Indian Ocean stations; (b) sites in equatorial Americas; (c) eastern South America,
995 Ascension, Nairobi. Station mean profiles are from 1998-2016, except for Costa Rica and
996 Hanoi, where launches started in 2004 and 2005, respectively.

997

Station Name	Location	Local Launch Times*	Ground Total Ozone Instr.	Profile #	Reprocessing Reference
Am. Samoa	14.23S, 170.56W	0800 – 1200, 1300 - 1800	Dobson #80	480	Sterling17
Hilo, Hawaii	19.40N, 155.0W	0800 - 1300	---	600	Sterling17
San Cristóbal, Galapagos (Ecuador)	0.92S, 89.60W	0500 - 1700	---	387	Sterling17
Costa Rica (various sites)**	9.94N, 84.04W	0600 - 1200	---	440	Witte17, This study
Paramaribo, Surinam	5.81N, 55.21W	0900 - 1400	Brewer #159	476	Allaart et al., in prep., <i>AMT</i>
Ascension Is., UK	7.98S, 14.42W	1300 - 1400	---	538	Witte17a
Natal, Brazil	5.42S, 35.38E	1200 - 1400	Dobson #93	517	Witte17a
Irene, South Africa	25.9S, 28.22E	1000 - 1300	Dobson #89	258	Witte17a
Nairobi, Kenya	1.27S, 36.80E	0700 - 1800	Dobson #18	719	Witte17b
La Réunion, France	21.1S, 55.48E	0800 - 1300	SAOZ#20	521	Witte17a,b with modification described in Sec 2.2.
Kuala Lumpur, Malaysia	2.73N, 101.7E	1000 - 1200	Brewer #90	271	Witte17a
Hanoi, Vietnam	21.02N, 105.80E	1300 - 1400	Brewer #208	148	Witte17a
Watakosek-Java, Indonesia	7.57S, 112.65E	1200 - 1300	Brewer #116 in Bandung	146	Witte17a
Suva, Fiji	18.13S, 112.65E	0800 – 1100, 2100 - 2300	--	222	Sterling17

*On average times.

** Current site is San Pedro. Alajuela and Heredia historic sites are within 0.5 degrees of San Pedro.

Table 1. SHADOZ stations with co-located ground-based total ozone instrument (where applicable) and sample numbers (total reprocessed records with bursts between 10-15 hPa). Reference for reprocessing is also given.

Table 2. Radiosondes used at SHADOZ stations

	RS80 or RS92	Pressure Offset Correction	iMet	Pressure Offset Correction
Samoa	RS80: 1998 - 2013	No	2014/01/10 – present	Yes
Fiji	RS80: 1998 - 2013	Intermittent	2015 – present	Yes
Hilo	RS80: 1998 – 2012/09/05	Intermittent – yes after 2009/04/08	2012/09/12 – 2012/11/28	No
			2012/12/05 - present	Yes
San Cristóbal	RS80: 1998 – 2008	No	---	---
	RS92: 2012/05 – present	Yes		
Costa Rica*	RS80: 2005 - 2013/08/16	Yes – Vömel method**	2010/08/19 - present	Yes
Paramaribo	RS80: 1999 – 2005/09/17	No	---	---
	RS92: 2005/10/03 – present			
Nairobi	RS80: 1998 – 2010/03/03	No	---	---
	RS92: 2010/06/09 - present			
Ascension			2016 – present***	Yes

*Overlap of iMet and RS80 between 2010/08 – 2013/08

** Using rise rate

***LMS: 1998 – 2010 (refer to Wittel7a)

Table 3. The mean and 1-sigma standard deviations of TCO, stratospheric, and tropospheric O₃, the latter from the sondes. Values are reported in units of DU. TCO are reported from satellite, ground-based, and ozonesonde instruments. Column 4 includes the percent difference of sonde and satellite mean TCO with respect to sondes. Stratospheric O₃ includes the residual climatology. Sites within ±19 degree of the equator itemized first from west to east to show the tropospheric wave-one amplitude (column 6). Sub-tropical sites follow.

Site	Satellite TCO*	Ground-based TCO	Sonde TCO (mean Sat. Δ, %)	Sonde Strat. O ₃	Sonde Trop O ₃	Tropopause [hPa]
Tropical Sites within ±19° of Equator						
Samoa	251.7±11.0	248.0±10.1	249.4±12.1 (-0.9)	227.9±9.7	21.6±6.3	94.5±13.2
San Cristobal	260.4±12.1	--	258.2±15.0 (-0.9)	231.2±11.9	27.5±10.8	90.6±16.3
Costa Rica	255.7±14.34	--	255.3±19.2 (-0.2)	229.4±17.2	26.0±5.4	94.8±27.4
Paramaribo	262.1±13.8	260.3±12.7	273.0±19.0 (+4.0)	242.1±15.2	30.1±6.8	96.7±22.1
Natal	265.4±11.3	268.8±12.7	260.9±15.1 (-1.7)	226.6±10.1	34.3±8.1	92.9±9.9
Ascension	266.7±10.4	--	260.4±17.9 (-2.4)	221.5±12.5	38.6±8.4	92.8±15.8
Nairobi	260.1±12.4	257.9±13.7	255.8±11.3 (-1.7)	227.2±9.4	28.6±4.9	90.0±14.7
Kuala Lumpur	259.5±13.4	256.6±22.3	246.0±13.5 (-5.5)	220.1±12.8	26.0±5.8	93.3±10.3
Watakosek	257.5±9.5	250.4±10.4	254.3±10.9 (-1.3)	226.9±8.7	27.2±6.8	88.4±8.2
Fiji	258.4±14.5	--	256.0±16.0 (-0.9)	231.0±11.2	24.6±7.9	93.9±11.9
Sub-Tropical Sites						
Hilo	273.7±18.4	--	270.4±20.3 (-1.2)	238.8±17.7	31.9±8.0	117.5±41.2
Irene	268.1±15.9	274.6±17.3	273.6±20.0 (+2.0)	237.4±17.3	36.2±6.7	124.5±35.8
La Reunion	267.1±15.1	266.6±14.1	264.8±18.0 (-0.9)	229.6±13.2	35.5±7.8	103.3±25.8
Hanoi	264.7±17.6	276.2±17.6	261.7±21.1 (-1.2)	220.3±18.2	41.2±7.7	91.7±10.8

*Includes TOMS, OMI, OMPS TCO overpasses.

Figure 1.



Figure 2.

Ozone Measuring Satellites

past satellites
operating satellites
future satellites

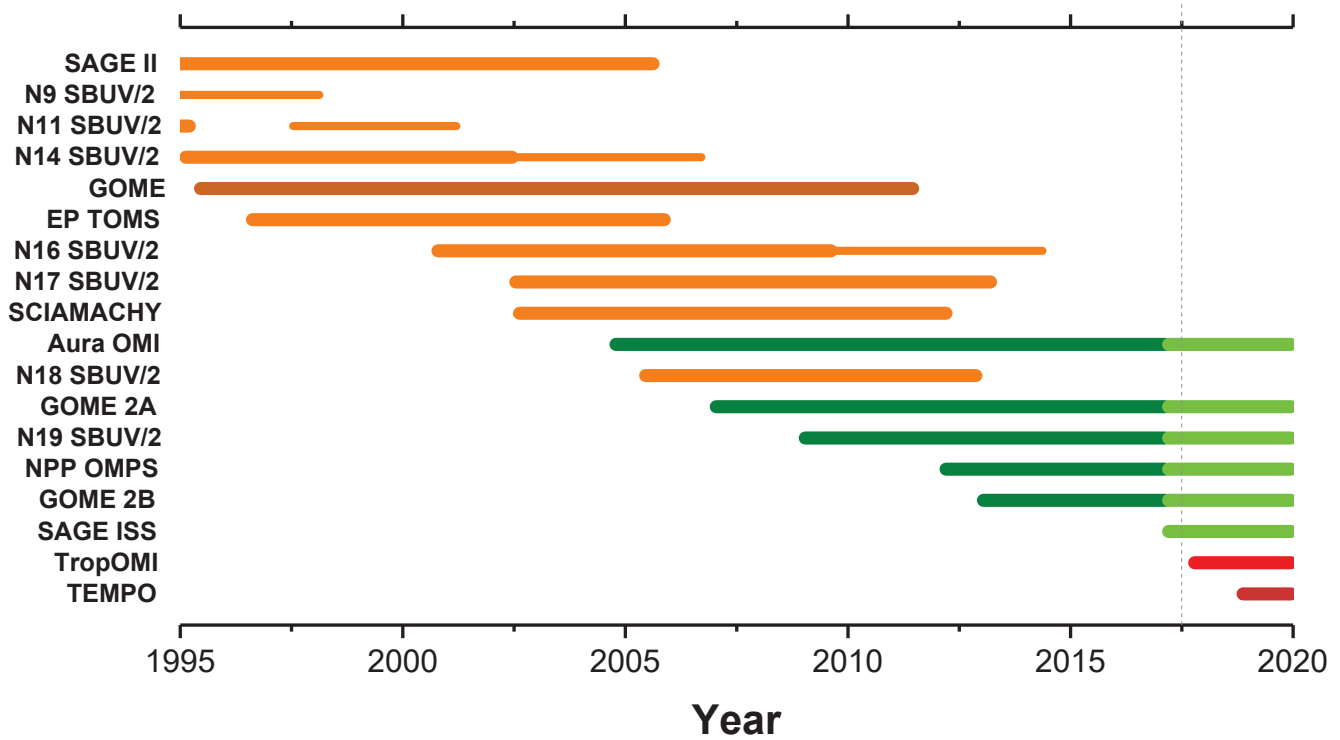


Figure 3.

Tropopause Heights

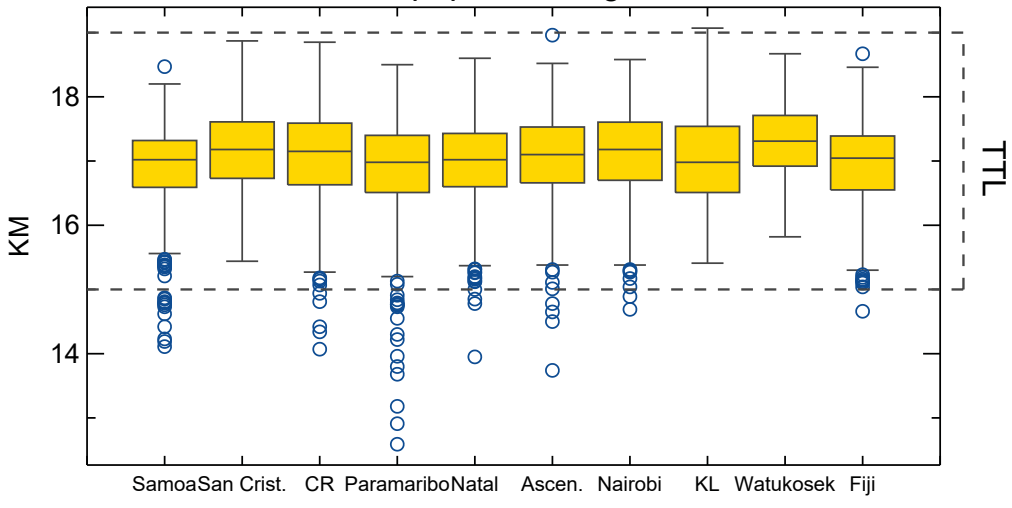
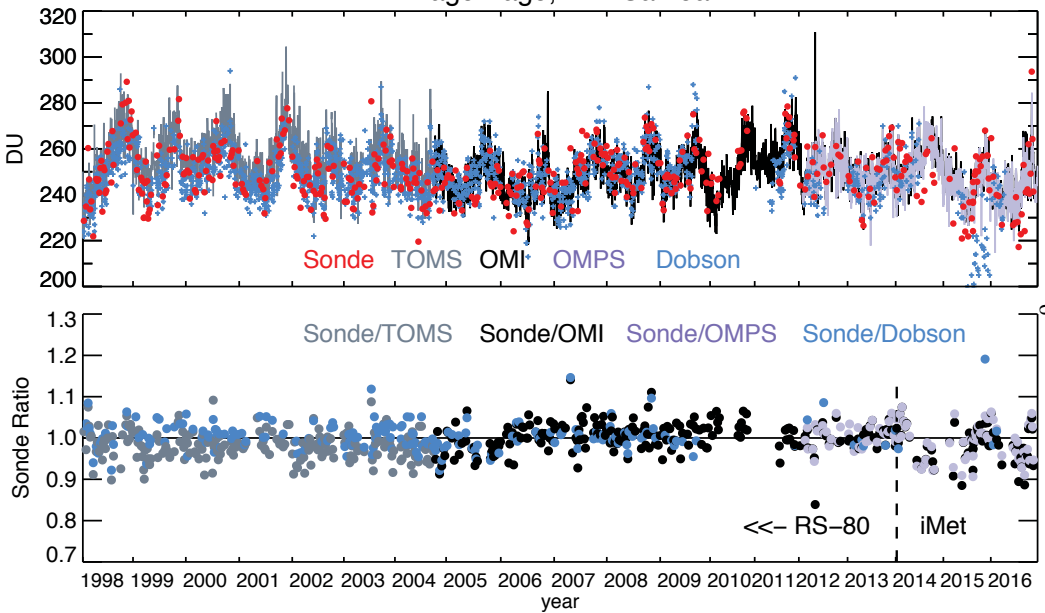


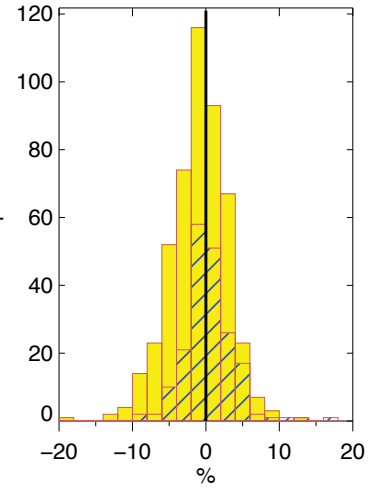
Figure 4.

a

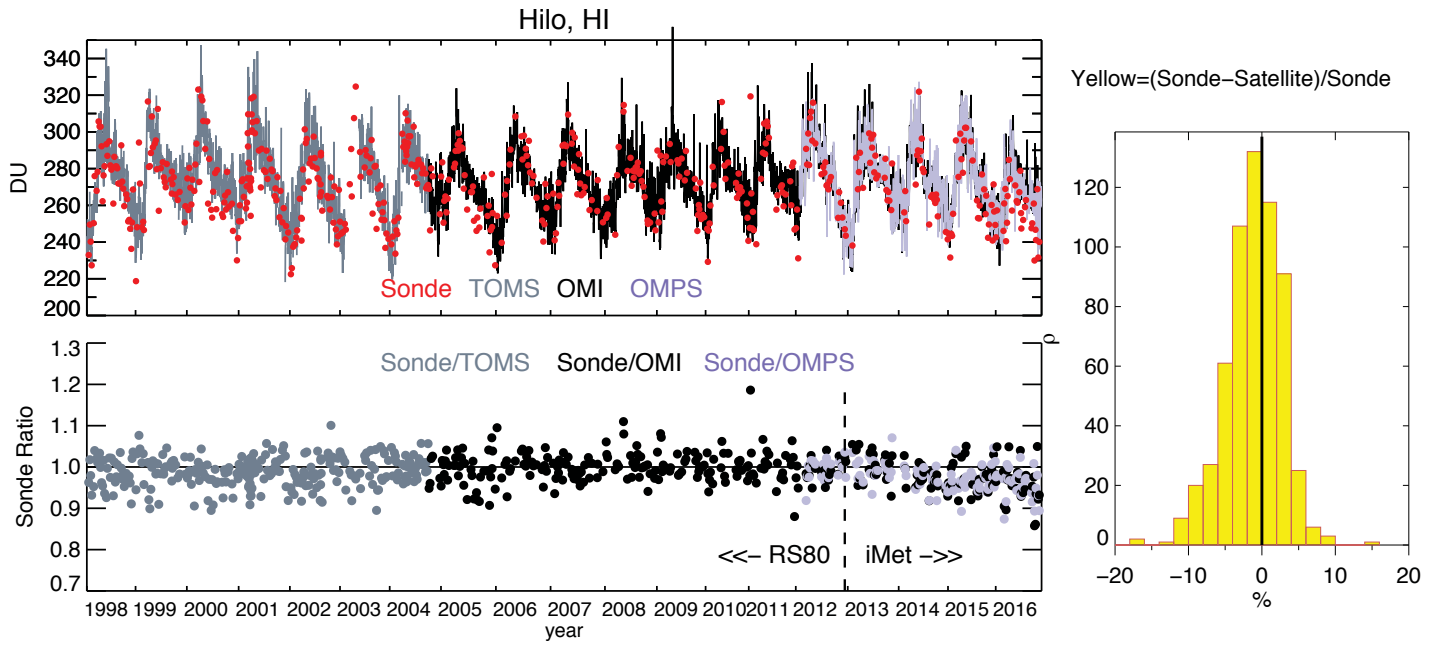
Pago Pago, Am. Samoa



Yellow= $(\text{Sonde} - \text{Satellite}) / \text{Sonde}$
Hash= $(\text{Sonde} - \text{Dobson}) / \text{Sonde}$

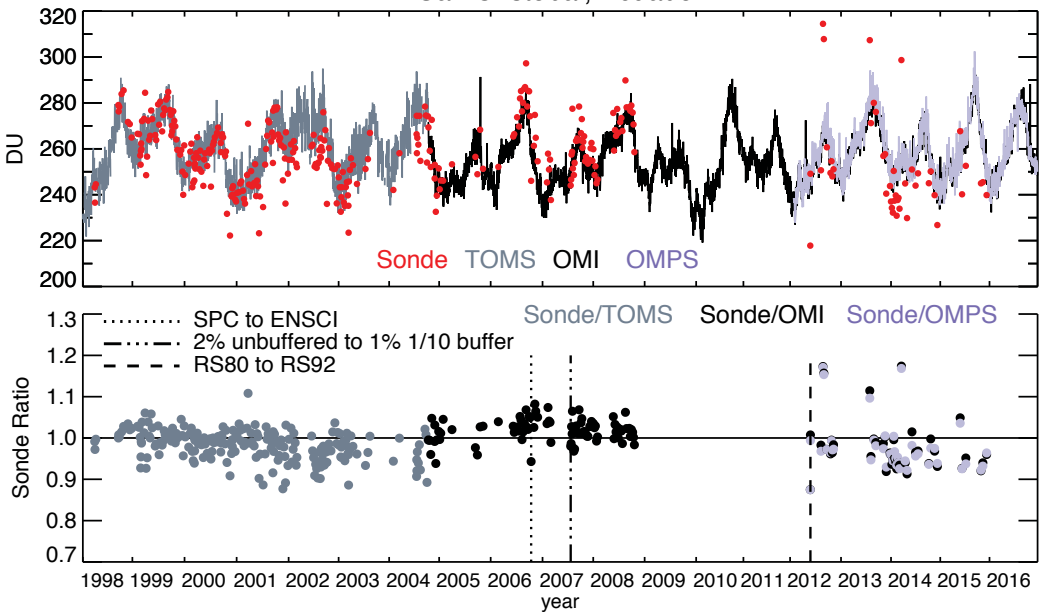


b

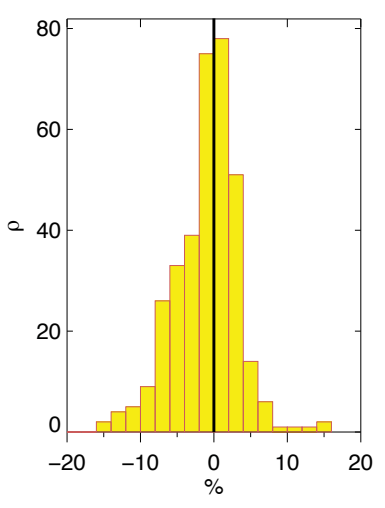


C

San Cristobal, Ecuador

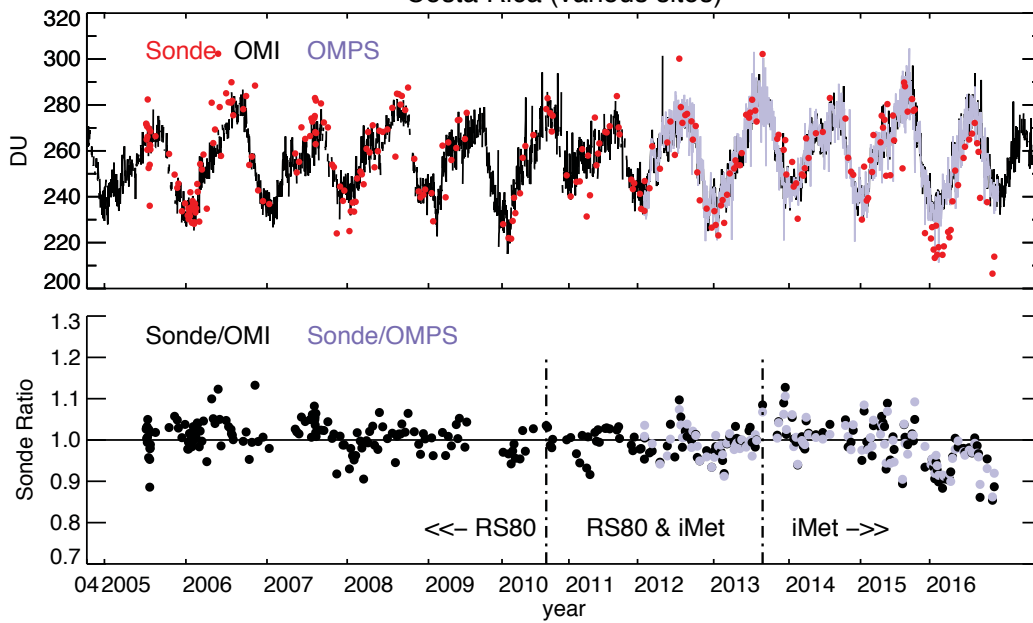


Yellow= $(\text{Sonde} - \text{Satellite}) / \text{Sonde}$

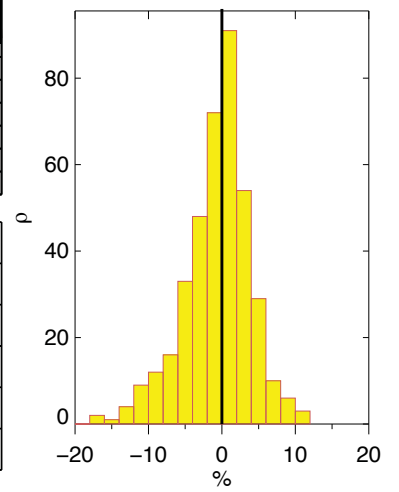


d

Costa Rica (various sites)

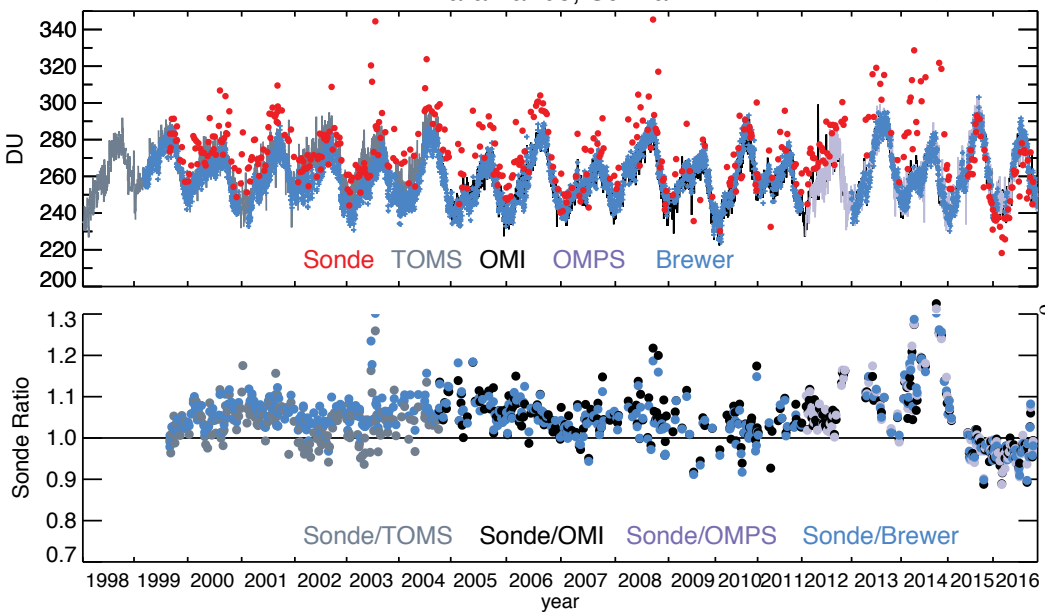


Yellow= $(\text{Sonde} - \text{Satellite}) / \text{Sonde}$

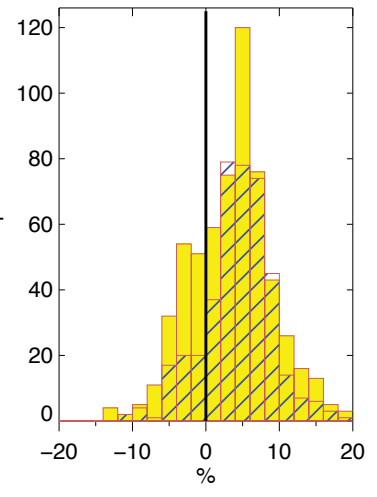


e

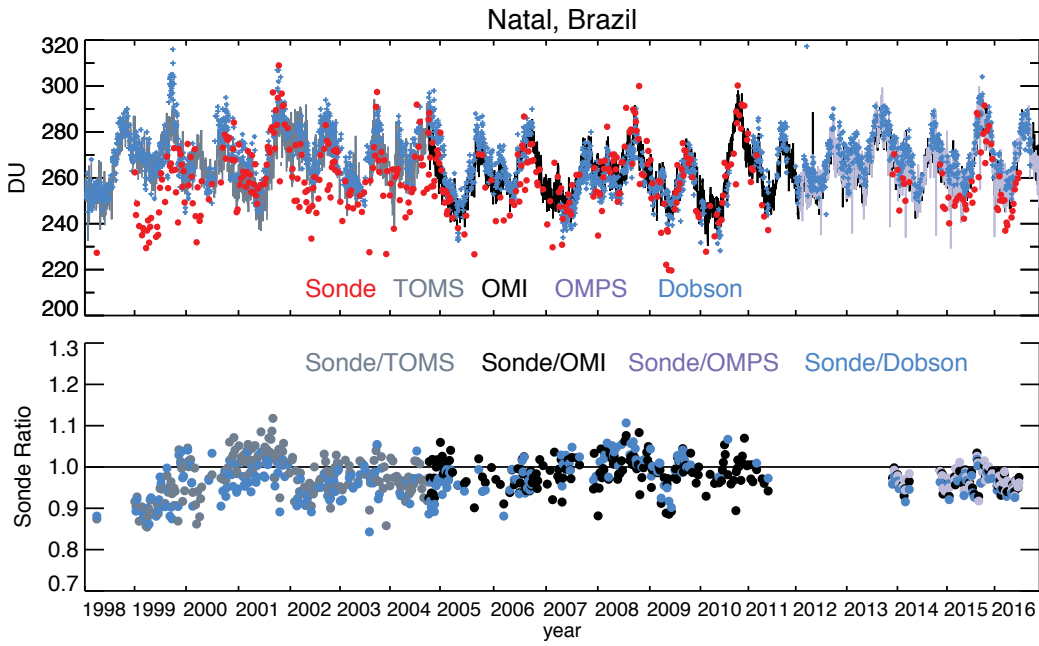
Paramaribo, Surinam



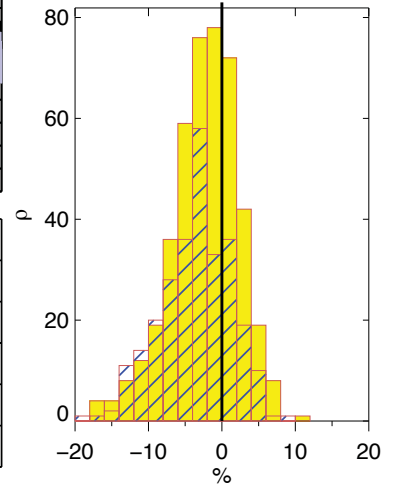
Yellow= $(\text{Sonde} - \text{Satellite}) / \text{Sonde}$
Hash= $(\text{Sonde} - \text{Brewer}) / \text{Sonde}$



f

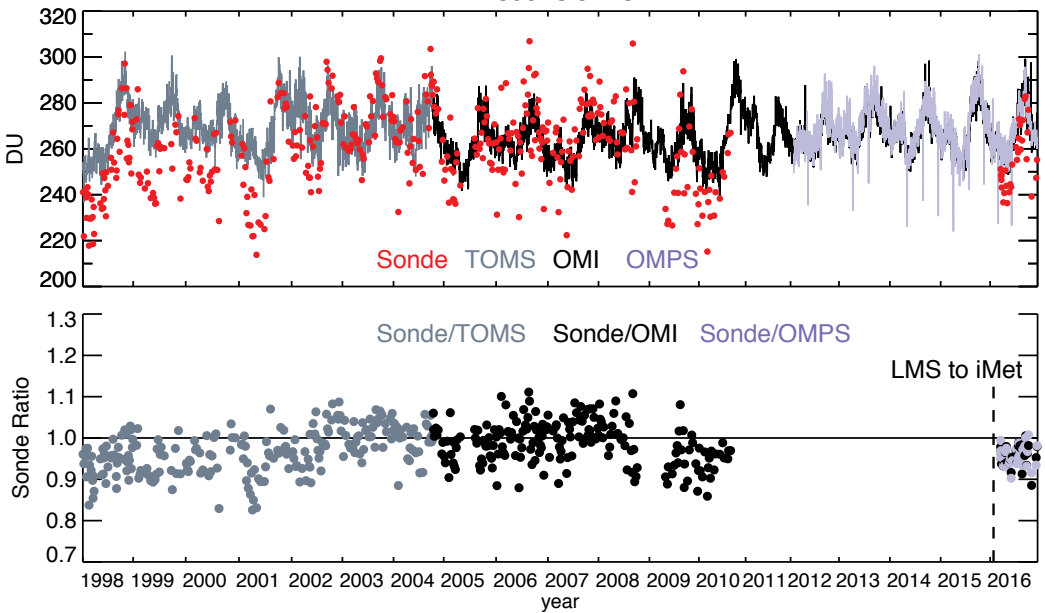


Yellow= $(\text{Sonde} - \text{Satellite}) / \text{Sonde}$
Hash= $(\text{Sonde} - \text{Dobson}) / \text{Sonde}$

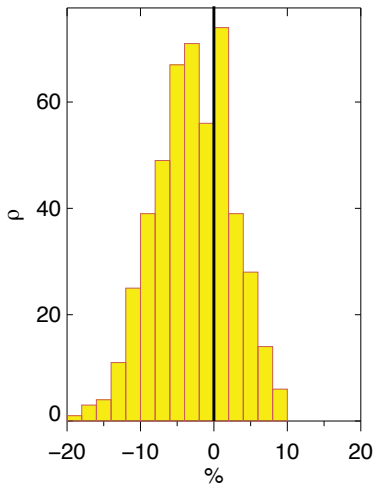


g

Ascension Is.

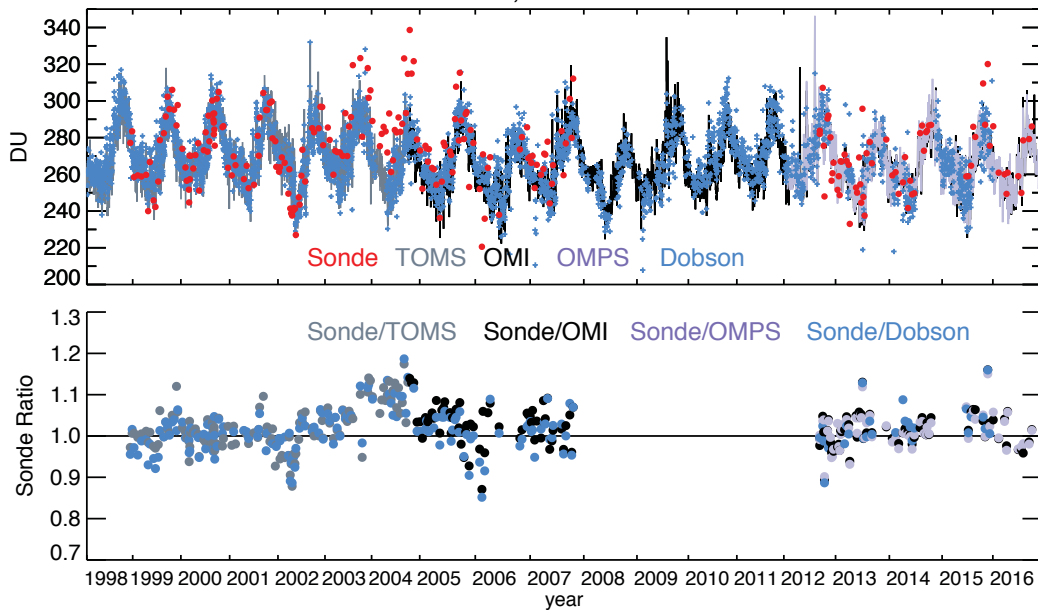


Yellow= $(\text{Sonde} - \text{Satellite}) / \text{Sonde}$

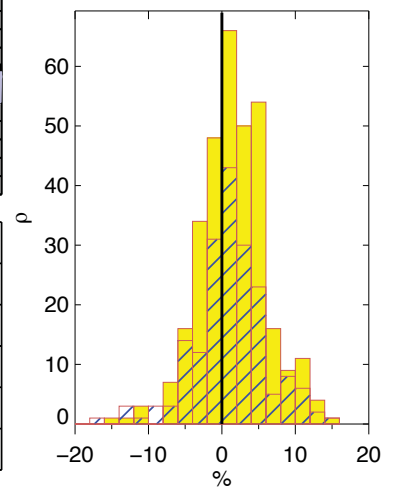


h

Irene, South Africa

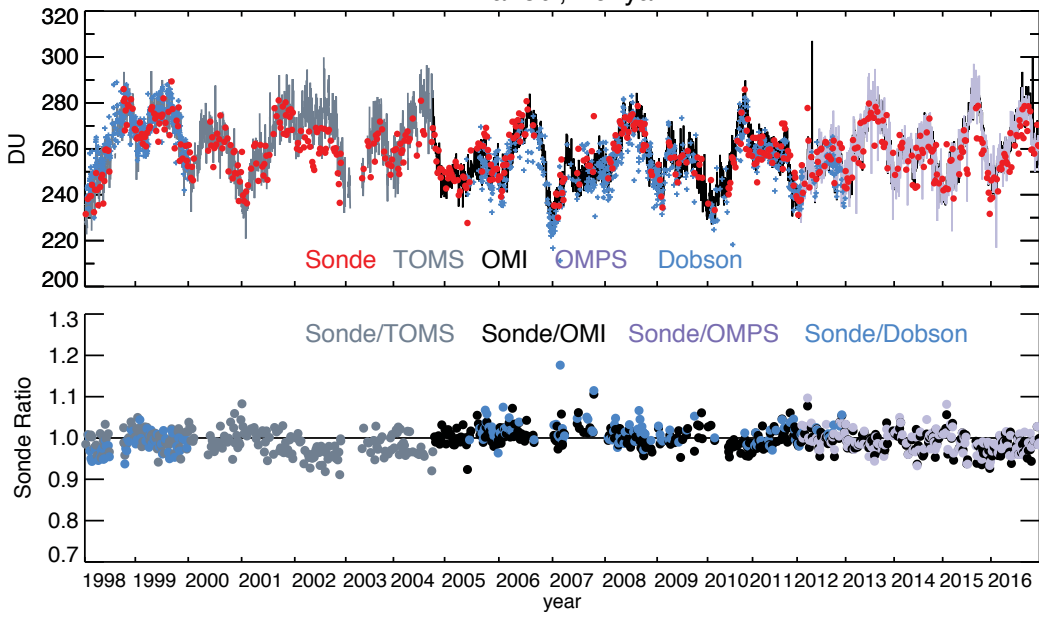


Yellow= $(\text{Sonde}-\text{Satellite})/\text{Sonde}$
Hash= $(\text{Sonde}-\text{Dobson})/\text{Sonde}$

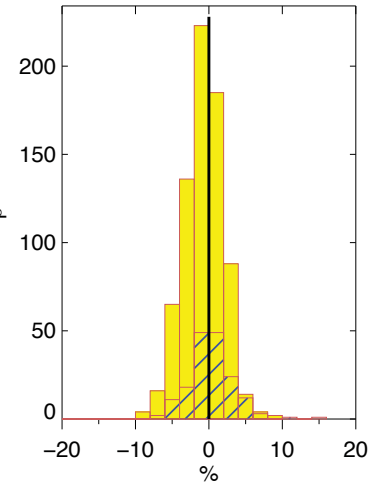


i

Nairobi, Kenya

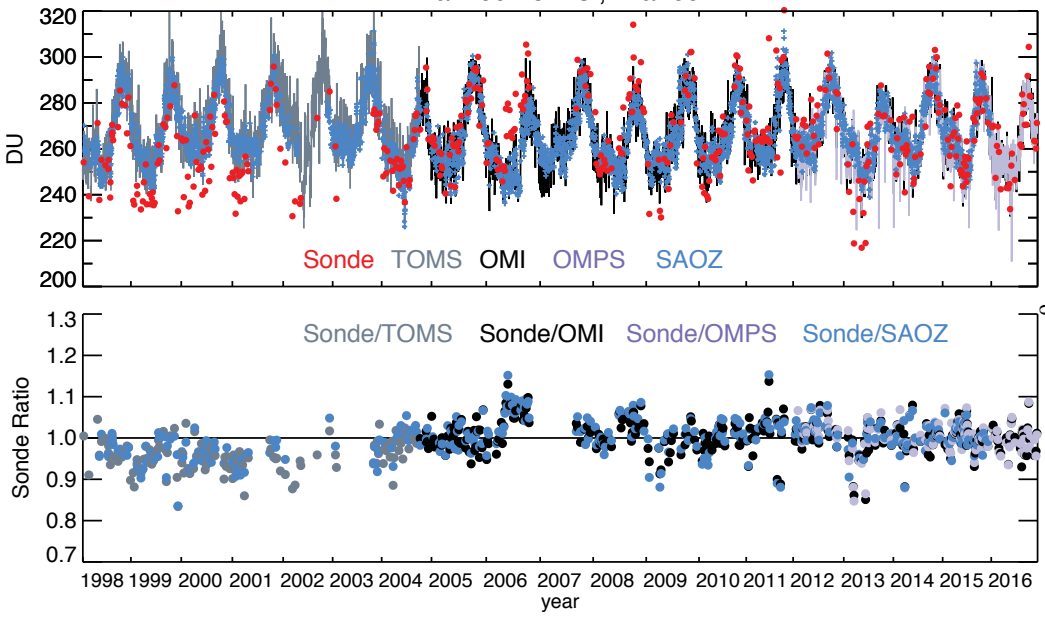


Yellow= $(\text{Sonde} - \text{Satellite}) / \text{Sonde}$
Hash= $(\text{Sonde} - \text{Dobson}) / \text{Sonde}$

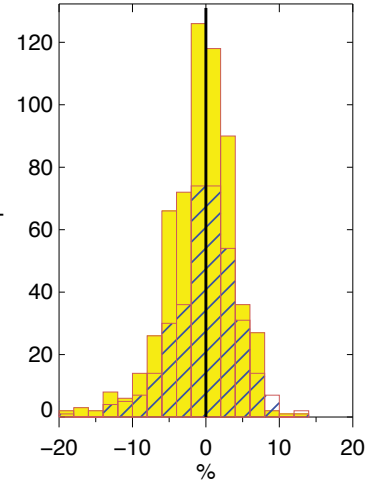


j

La Reunion Is., France

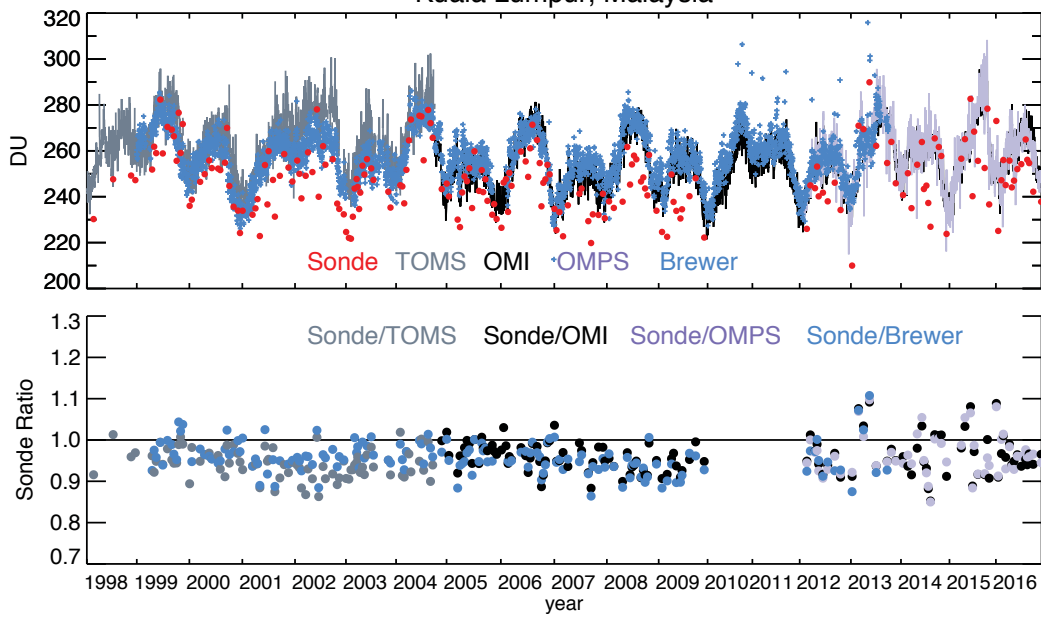


Yellow= $(\text{Sonde} - \text{Satellite}) / \text{Sonde}$
Hash= $(\text{Sonde} - \text{SAOZ}) / \text{Sonde}$

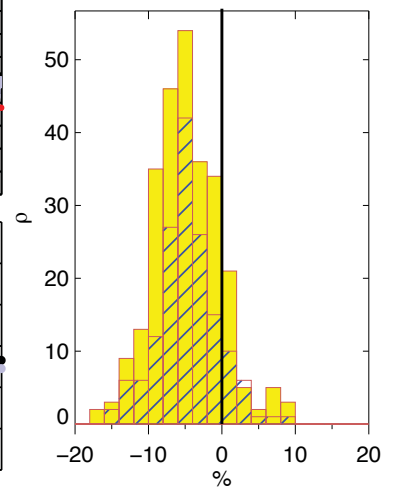


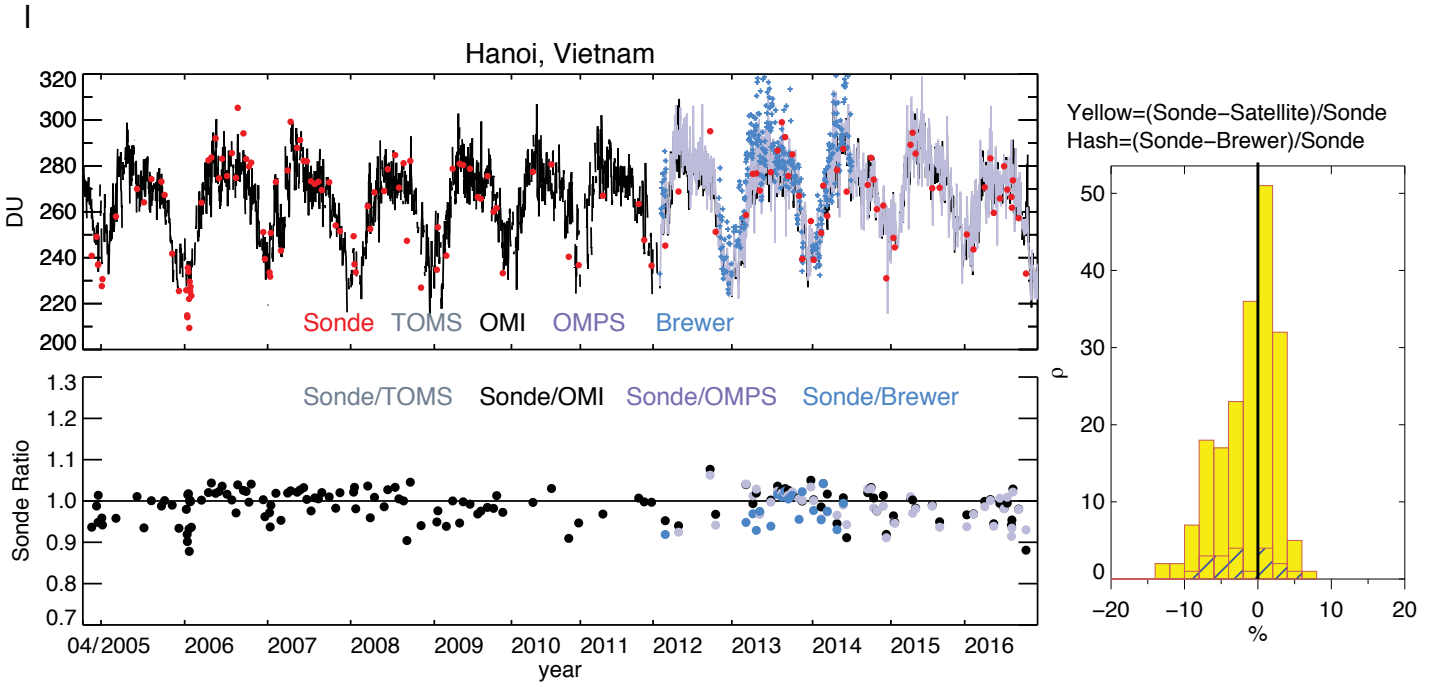
k

Kuala Lumpur, Malaysia



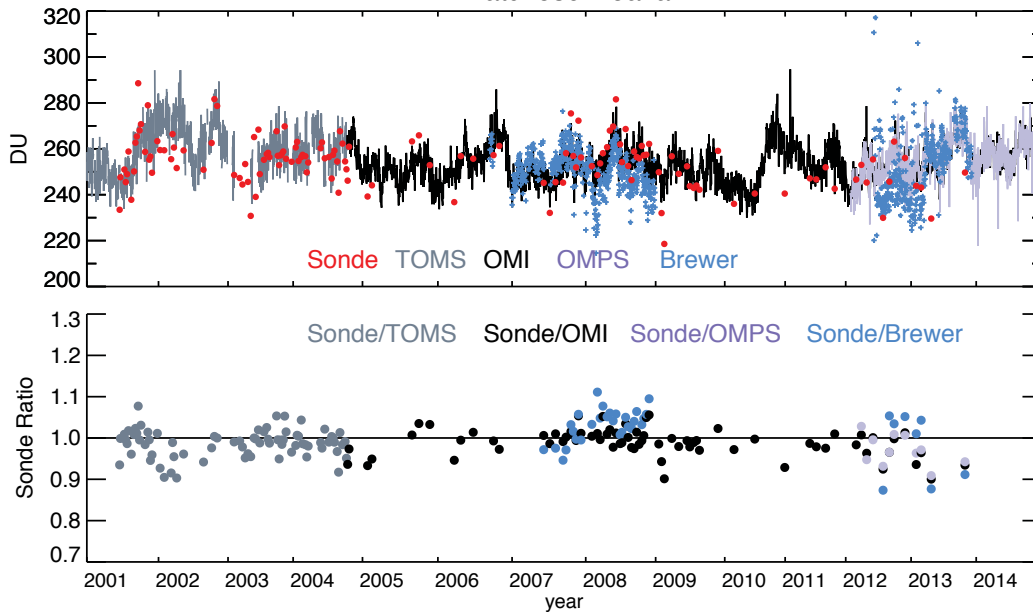
Yellow= $(\text{Sonde} - \text{Satellite}) / \text{Sonde}$
Hash= $(\text{Sonde} - \text{Brewer}) / \text{Sonde}$



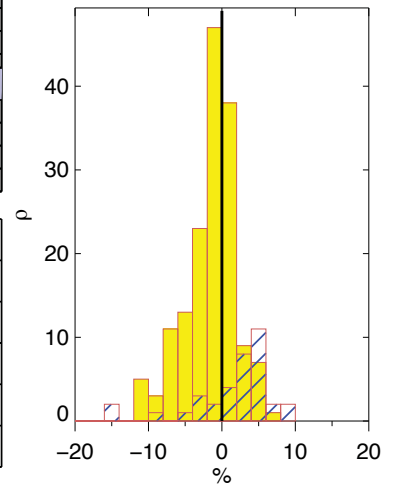


m

Watukosek-Java



Yellow= $(\text{Sonde}-\text{Satellite})/\text{Sonde}$
Hash= $(\text{Sonde}-\text{Brewer})/\text{Sonde}$



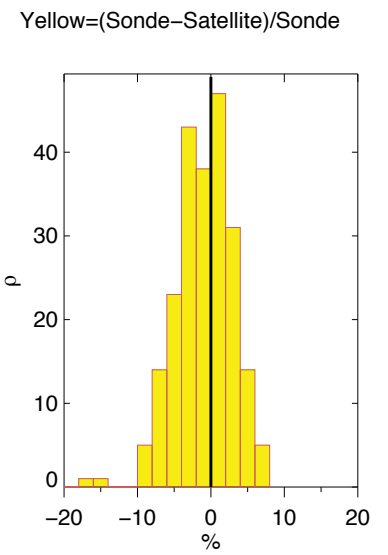
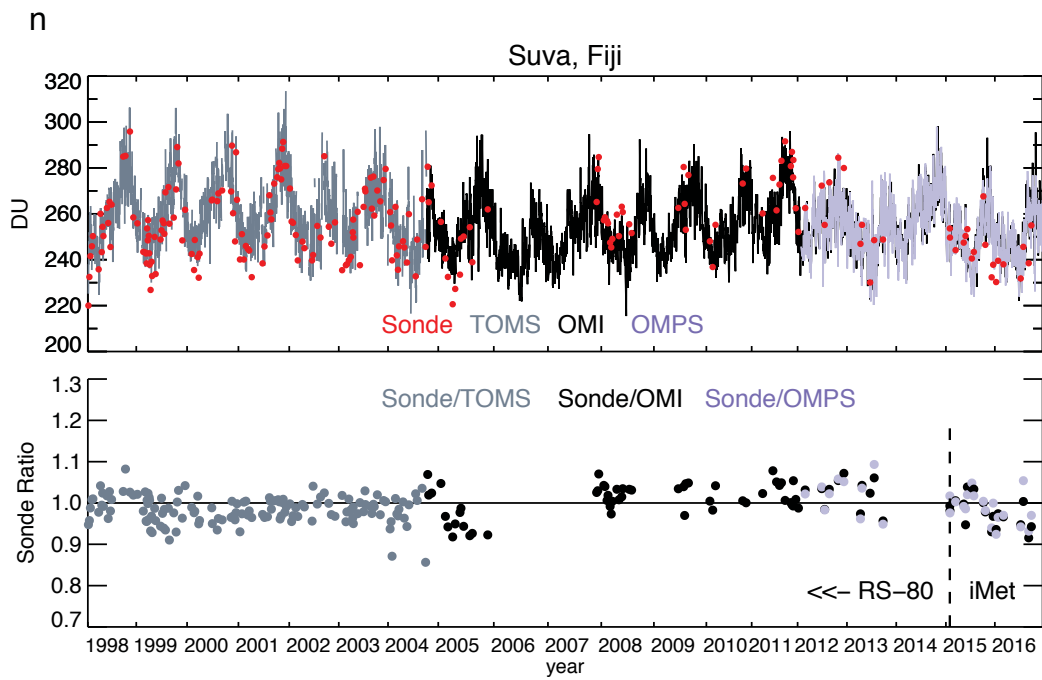
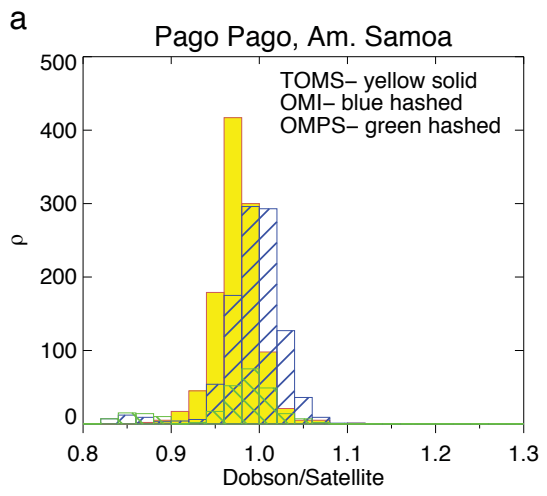
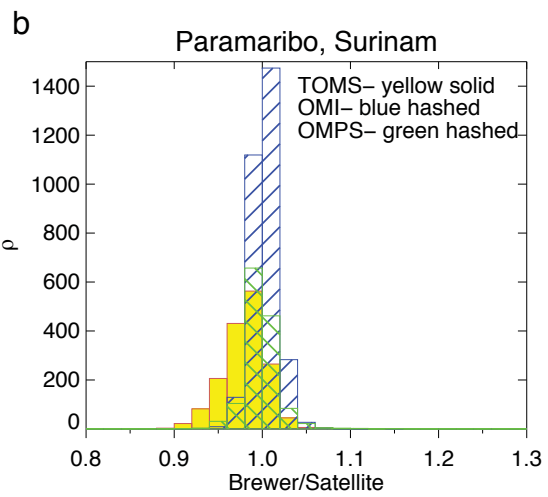
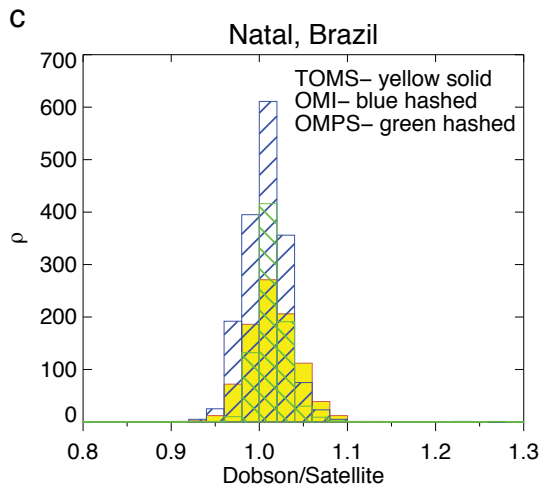
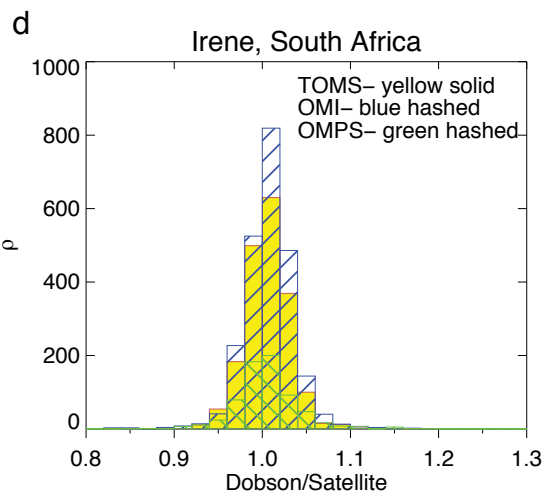


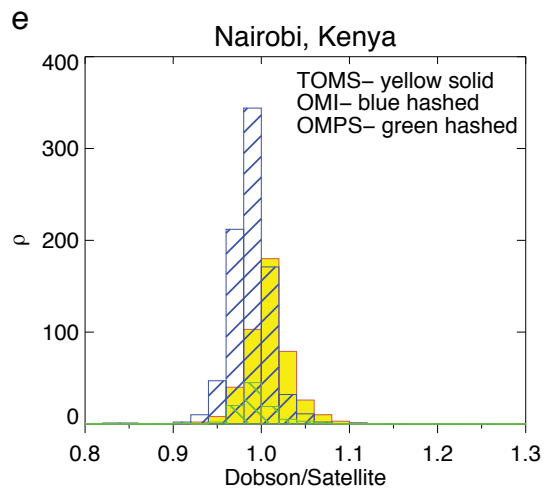
Figure 5.

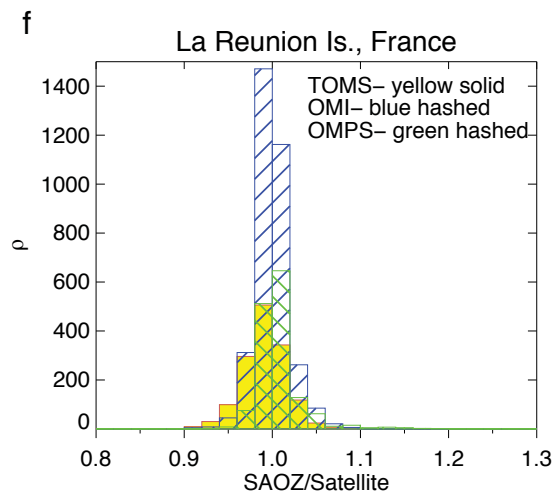


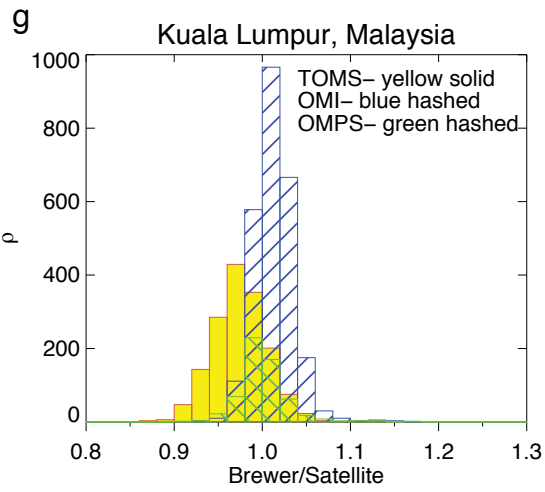


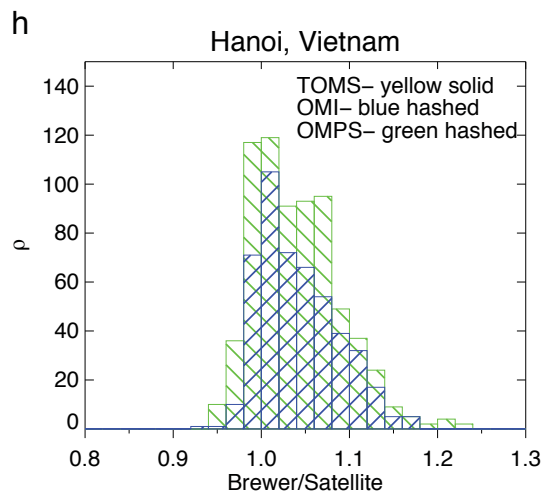












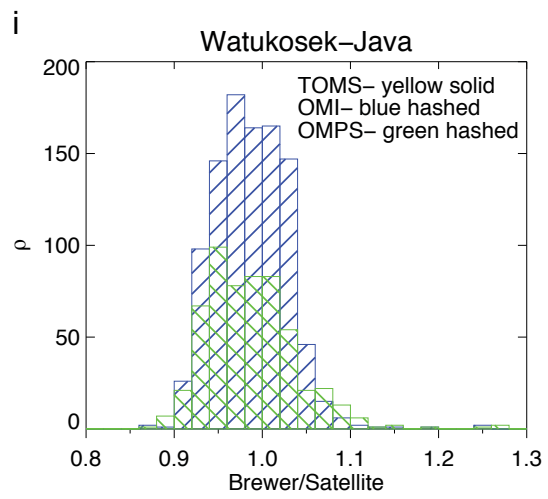


Figure 6.

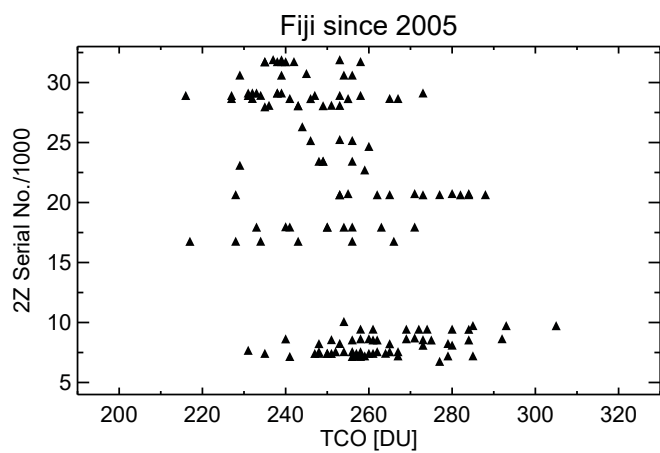
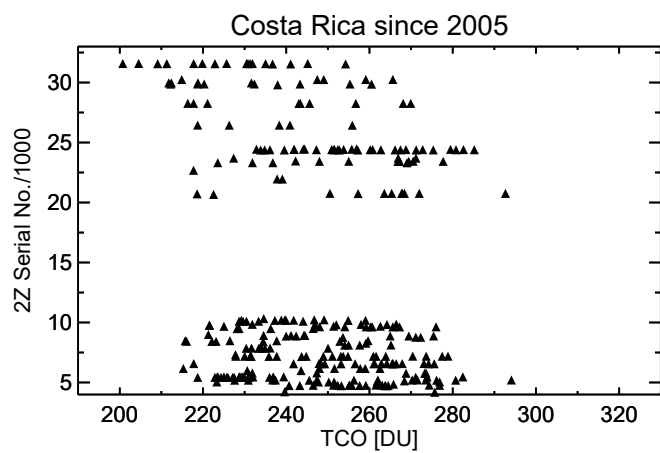


Figure 7.

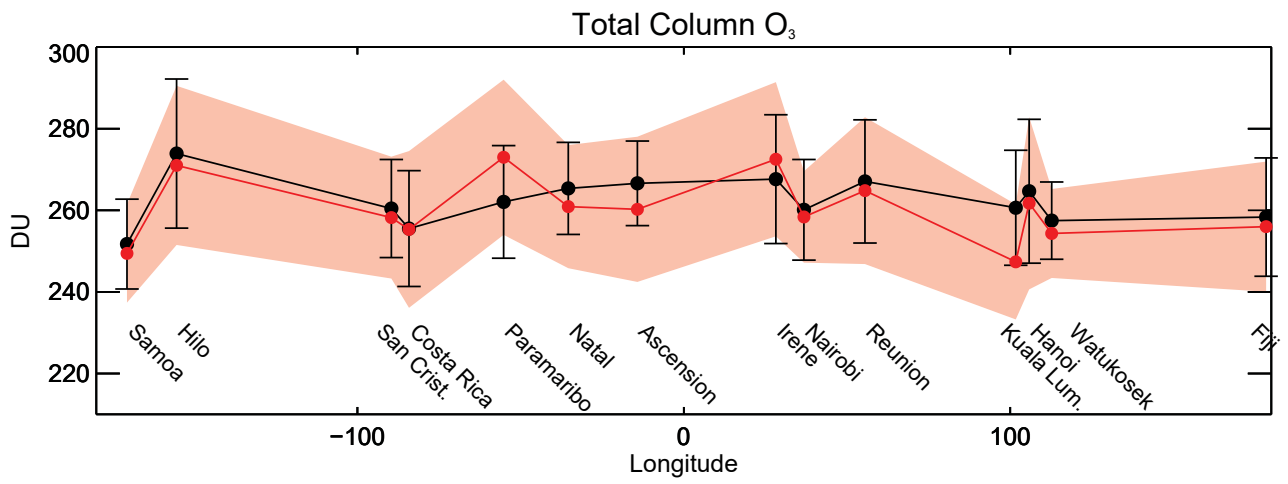
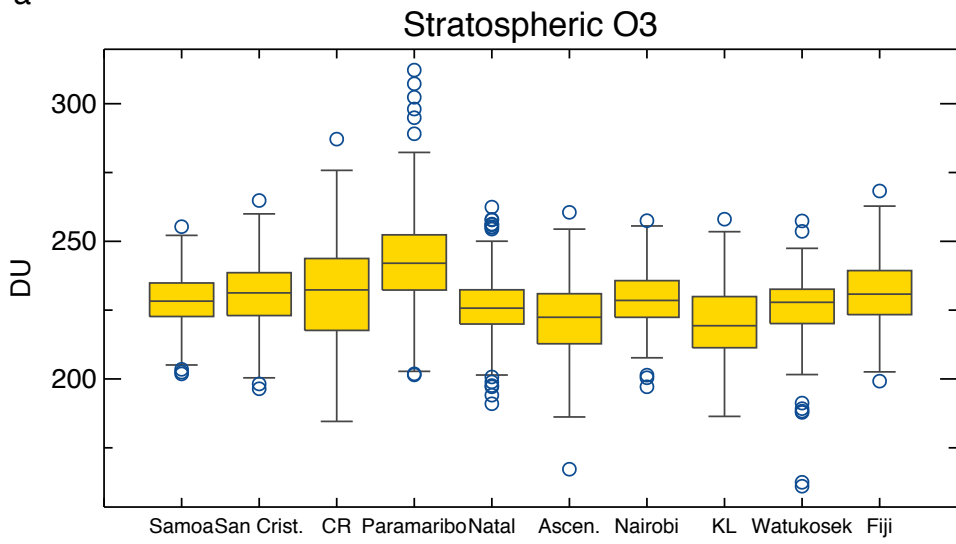
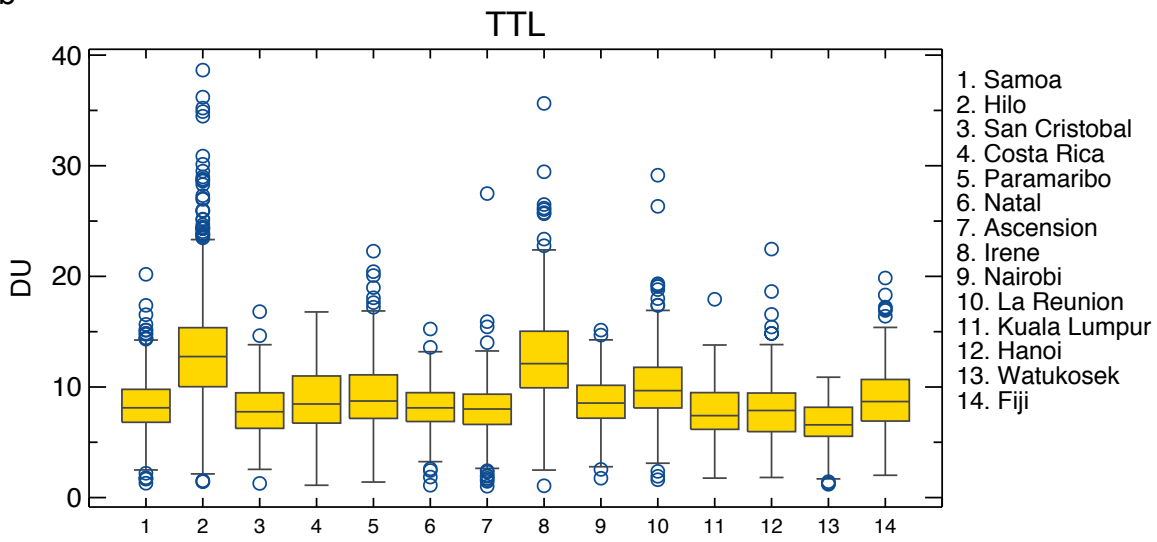


Figure 8.

a



b



c

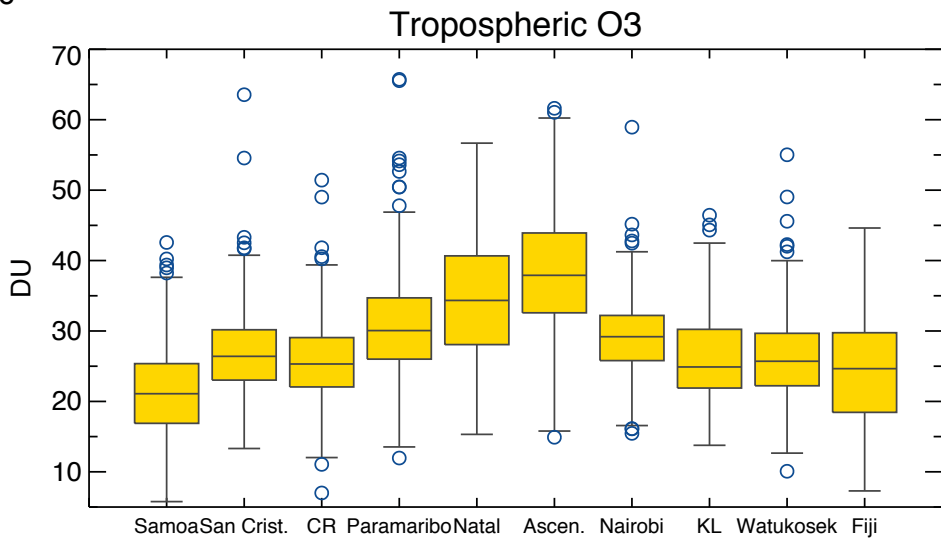


Figure 9.

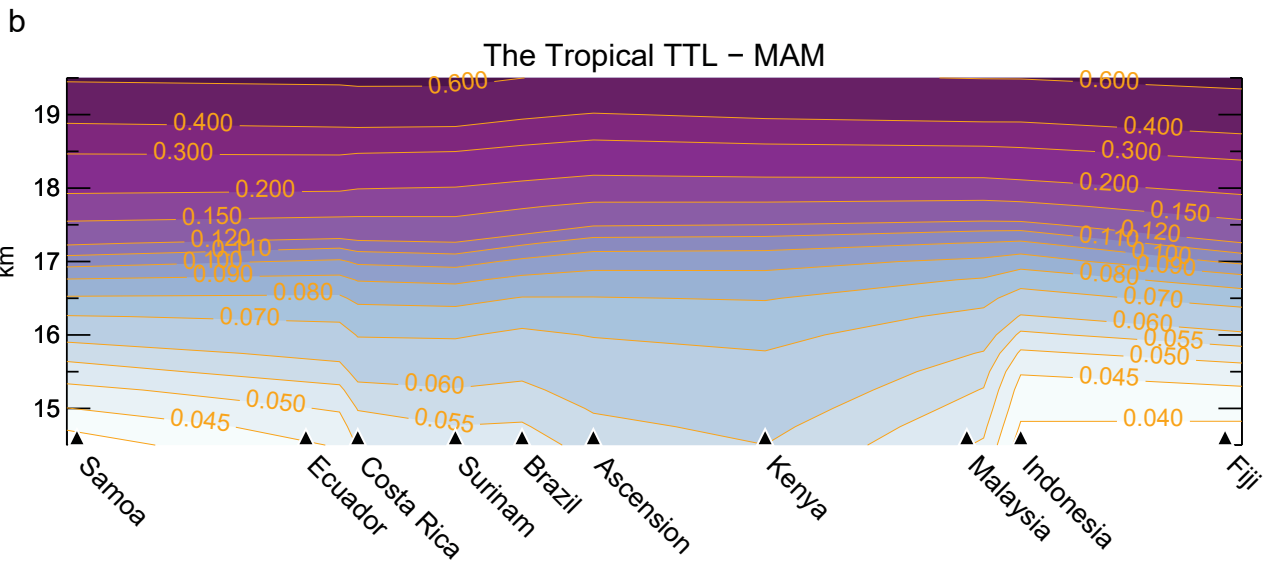


Figure 10.

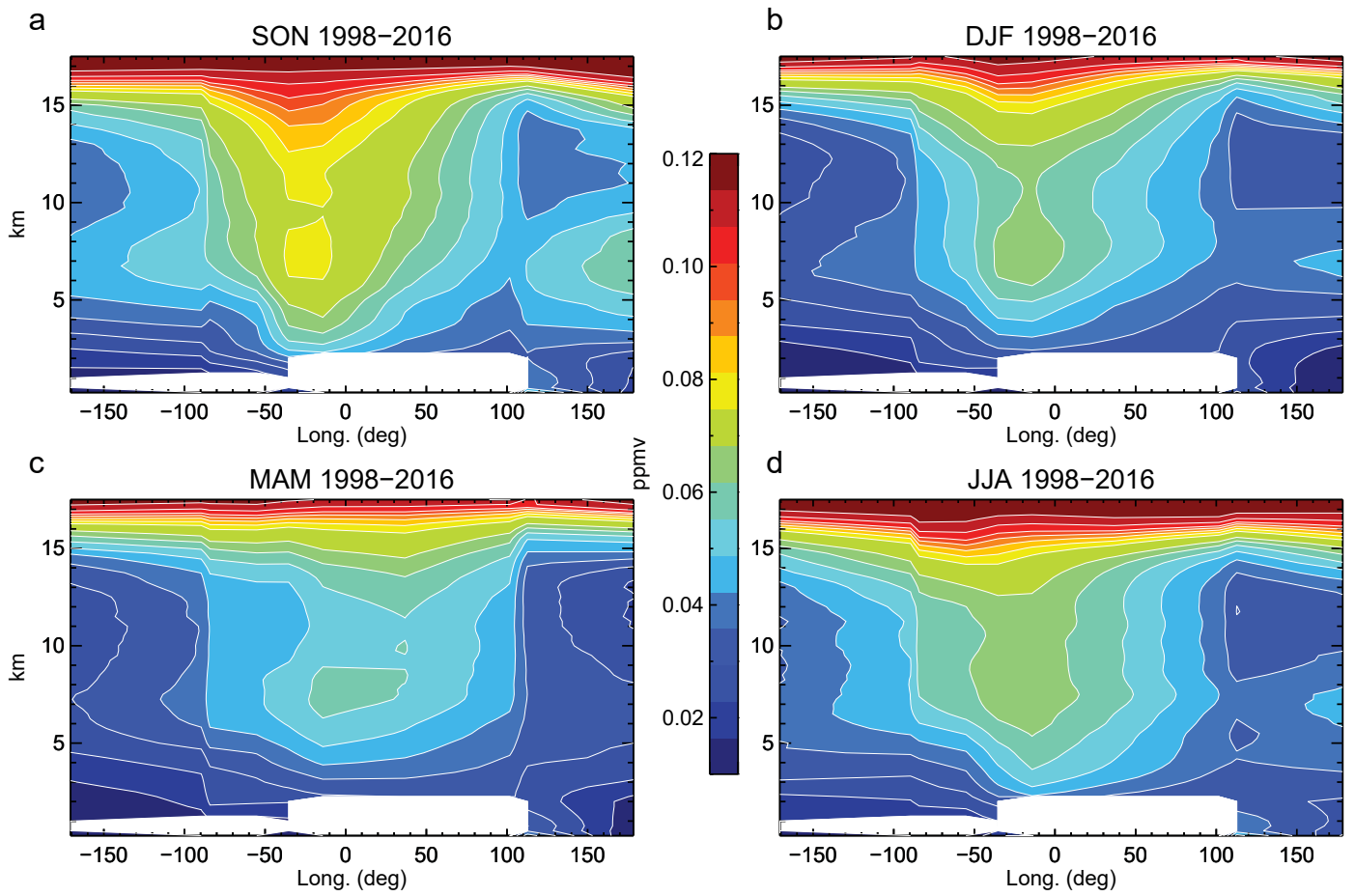


Figure 11.

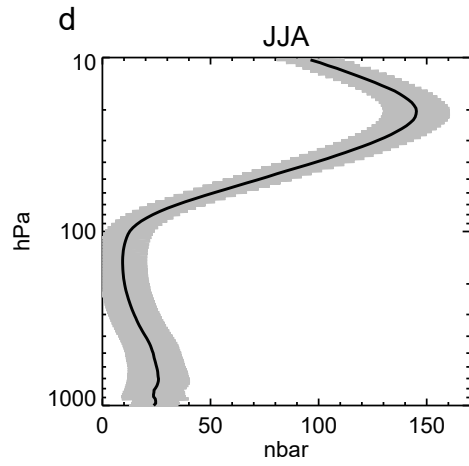
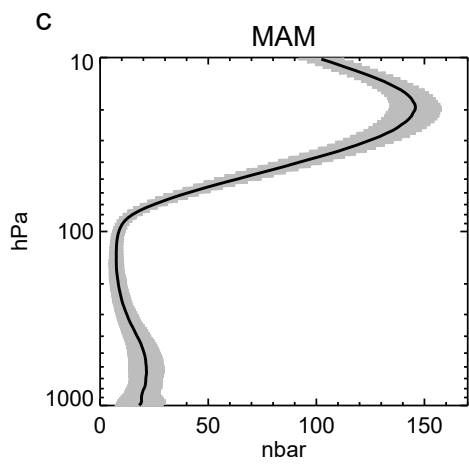
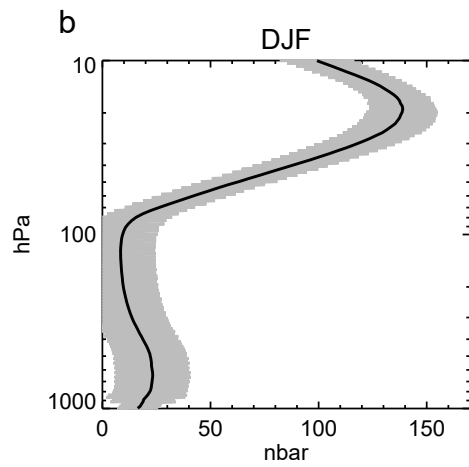
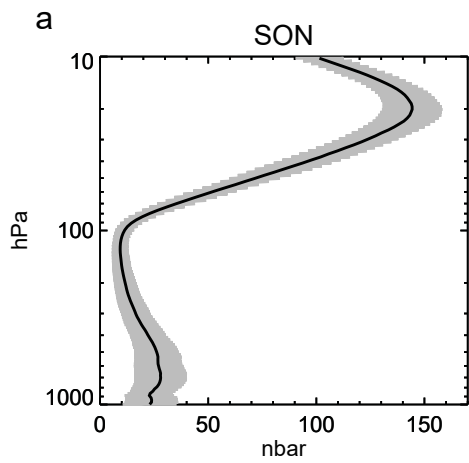


Figure 12.

